

Donor-Substituted 1,1,4,4-Tetracyanobutadienes (TCBDs): New Chromophores with Efficient Intramolecular Charge-Transfer Interactions by Atom-Economic Synthesis

Tsuyoshi Michinobu,^[a] Corinne Boudon,^[b] Jean-Paul Gisselbrecht,^[b] Paul Seiler,^[a] Brian Frank,^[a] Nicolle N. P. Moonen,^[a] Maurice Gross,^[b] and François Diederich*^[a]

Abstract: A wide variety of monomeric and oligomeric, donor-substituted 1,1,4,4-tetracyanobutadienes (TCBDs) have been synthesized by [2+2] cycloaddition between tetracyanoethylene (TNCE) and donor-substituted alkynes, followed by electrocyclic ring opening of the initially formed cyclobutenes. Reaction yields are often nearly quantitative but can be affected by the electron-donating power and steric demands of the alkyne substituents. The intramolecular charge-transfer (CT) interactions between the donor and TCBD acceptor moieties were comprehensively investigated by X-ray crystallography, electrochemistry, UV-visible spectroscopy, and theoretical calculations. Despite the nonplanarity of the new chromophores, which have a substantial twist between the two dicyanovinyl planes, efficient intramolecular CT interactions are observed, and the

crystal structures demonstrate a high quinoid character in strong donor substituents, such as *N,N*-dimethylanilino (DMA) rings. The maxima of the CT bands shift bathochromically upon reduction of the amount of conjugative coupling between strong donor and acceptor moieties. Each TCBD moiety undergoes two reversible, one-electron reduction steps. Thus, a tri-TCBD derivative with a 1,3,5-trisubstituted benzene core shows six reversible reduction steps within an exceptionally narrow potential range of 1.0 V. The first reduction potential $E_{\text{red},1}$ is strongly influenced by the donor substitution: introduction of more donor moieties causes an increasingly twisted TCBD

structure, a fact that results in the elevation of the LUMO level and, consequently, a more difficult first reduction. The potentials are also strongly influenced by the nature of the donor residues and the extent of donor–acceptor coupling. A careful comparison of electrochemical data and the correlation with UV-visible spectra made it possible to estimate unknown physical parameters such as the $E_{\text{red},1}$ of unsubstituted TCBD (−0.31 V vs Fc^+/Fc) as well as the maxima of highly broadened CT bands. Donor-substituted TCBDs are stable molecules and can be sublimed without decomposition. With their high third-order optical nonlinearities, as revealed in preliminary measurements, they should become interesting chromophores for ultra-thin film formation by vapor deposition techniques and have applications in opto-electronic devices.


Keywords: charge transfer • conjugation • cycloaddition • donor–acceptor systems • electrochemistry

Introduction

Donor–acceptor (D–A)-substituted conjugated organic molecules have attracted much attention for their highly polarizable structures and the resulting efficient second- and third-order nonlinear optical (NLO) effects.^[1] One of the most noticeable advantages of using organic chromophores is the ability to tune the physical properties and to enhance a specific NLO effect by simply modifying the chemical structure. In the past decade, a number of structure–NLO property relationships were established for various classes of conjugated organic molecules by changing conjugation length, as well as donor and acceptor strength and substitu-

[a] Dr. T. Michinobu, P. Seiler, B. Frank, Dr. N. N. P. Moonen, Prof. Dr. F. Diederich
Laboratorium für Organische Chemie, ETH-Hönggerberg
HCI, 8093 Zürich (Switzerland)
Fax: (+41) 1-632-1109
E-mail: diederich@org.chem.ethz.ch

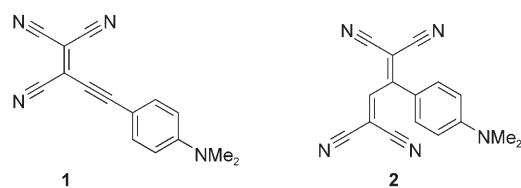
[b] Dr. C. Boudon, Dr. J.-P. Gisselbrecht, Prof. Dr. M. Gross
Laboratoire d'Electrochimie et de Chimie Physique du Corps Solide
UMR 7512, C.N.R.S., Université Louis Pasteur
4, rue Blaise Pascal, 67000 Strasbourg (France)

 Supporting information for this article is available on the WWW under <http://www.chemeurj.org/> or from the author.

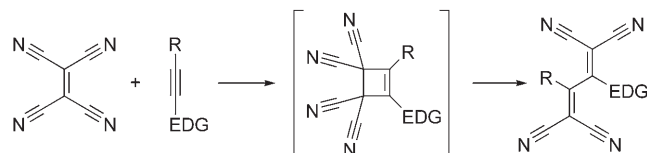
tion pattern.^[2] Well-defined guidelines to enhance the molecular first-order hyperpolarizability β were established, but definite principles for achieving high molecular second-order hyperpolarizability γ and high bulk NLO susceptibilities are still being pursued.

We have in the past shown that tetraethynylethenes (3,4-diethynylhex-3-ene-1,5-diynes, TEEs) substituted with *N,N*-dimethylanilino (DMA) donor and *p*-nitrophenyl acceptor groups feature high third-order optical nonlinearities, in particular in the case of low molecular symmetry.^[3] More recently, cyanoethynylethenes (CEEs), hybrid structures between TEEs and tetracyanoethylene (TCNE),^[4a,b] were proven to function as efficient acceptor groups for NLO applications if substituted with DMA donor groups.^[4c] As a distinct advantage over the corresponding TEE chromophores, DMA-substituted CEEs are more compact and can be sublimed without decomposition, thereby opening perspectives for opto-electronic device fabrication by ultra-thin film deposition.

TCNE is known as one of the strongest organic electron acceptors, and its high chemical reactivity towards nucleophiles or electron-rich reagents is frequently used to introduce strong acceptor moieties into organic molecules.^[5] For example, DMA-substituted tricyanomonoethynylethene **1**



was synthesized by nucleophilic addition–elimination reaction of TCNE with the corresponding copper(i) arylacetylide, prepared from 4-ethynyl-*N,N*-dimethylaniline and CuOAc.^[6] We have recently found that the same combination of initial starting materials, 4-ethynyl-*N,N*-dimethylaniline and TCNE, can also furnish a member of a new class of D–A chromophores, that is, DMA donor-substituted 1,1,4,4-tetracyanobuta-1,3-diene (TCBD) **2**.^[7] This atom-economic,^[8] one-step transformation proceeds in nearly quantitative yield by means of [2+2] cycloaddition between TCNE and the electron-rich alkyne followed by electrocyclic ring opening of the intermediately formed cyclobutene ring to give the TCBD framework (Scheme 1).



Scheme 1. Reaction between TCNE and an alkyne substituted with an electron-donating group (EDG) to yield the corresponding donor-substituted TCBD derivative.

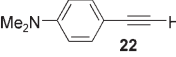
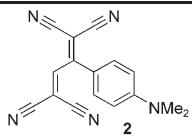
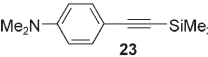
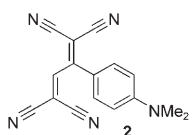
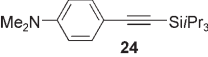
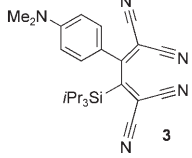
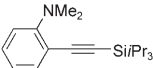
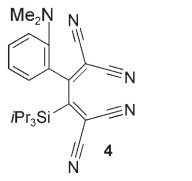
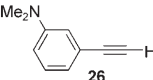
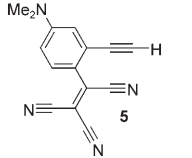
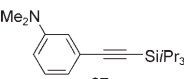
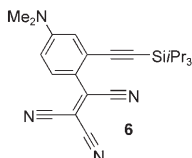
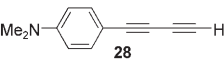
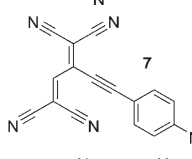
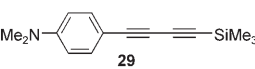
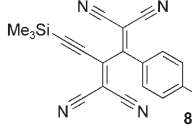
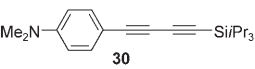
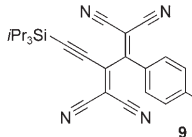
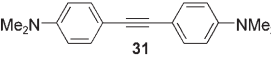
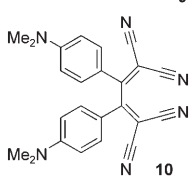
A variety of organic and organometallic TCBD-containing molecules have been reported before,^[9,10] and some of them have been investigated as second-order NLO materials, taking into account the nonplanar structure of the TCBD moieties. However, there has been no systematic study on their synthesis and electronic properties. Here, we describe the reactivity of a series of electron-rich alkynes towards TCNE and also report the synthesis of donor-substituted TCBD oligomers. Their electronic properties are characterized by X-ray crystallography, electrochemistry, optical absorption spectroscopy, and theoretical calculations. The data confirm that donor-substituted TCBDs, despite their nonplanarity, are powerful charge-transfer (CT) compounds with physical properties suitable for nonlinear optical applications^[7] and device fabrication.

Results and Discussion

Synthesis of monomeric donor-substituted tetracyanobutadienes: A variety of electron-rich alkynes (**22–42**) were prepared by Sonogashira cross-coupling or Hay coupling reactions (see Supporting Information) and subsequently subjected to the reaction with TCNE to give products **2–21** (Tables 1 and 2).

In the preparation of monomeric TCBDs, we first compared the reactivity of *o*-, *m*-, and *p*-*N,N*-dimethylanilino (DMA) derivatives **22–27** towards TCNE (entries 1–6, Table 1). Whereas the *p*-DMA-substituted, terminally deprotected alkyne **22** reacted at 20°C to give TCBD **2** in nearly quantitative yield (97%), the yield of the *i*Pr₃Si-protected product **3** was lower (78%), reflecting the steric hindrance from the *i*Pr₃Si group. Starting from Me₃Si derivative **23**, TCBD **2** was isolated in only 48% yield after chromatography, with silyl deprotection taking place on the weakly acidic SiO₂ support, as a result of the Si activation by the attached dicyanovinyl moiety. In contrast, the reactions of the *o*- and *m*-DMA-substituted alkynes with TCNE did not proceed at room temperature due to sterically reduced (*ortho*) or lacking (*meta*) electron-donating ability. Rather, heating to 70°C in the absence of solvent and in the presence of an excess of TCNE was necessary to accomplish transformation. Solvents such as CH₂Cl₂ are sometimes found to reduce the reaction yield, whereas an excess of TCNE does not induce undesired side reactions and is easily removed by sublimation and chromatography. The TCBD product from 2-ethynyl-*N,N*-dimethylaniline was too unstable to be isolated, but *i*Pr₃Si-protected TCBD **4** was obtained from the corresponding alkyne **25** in a yield of 27% (entry 4, Table 1). The low yield is derived from the limited chemical stability of the product which, in sharp contrast to highly stable **2** and **3**, completely decomposed after one day in the solid state at room temperature. *m*-DMA-substituted alkynes **26** and **27** did not undergo cycloaddition to TCNE; rather, tricyanovinylation occurred in *para* position of the aniline ring yielding the stable donor-substituted tricyanoethenes **5** and **6**, respectively, in good yield (68–69%; entries 5 and 6, Table 1).

Table 1. Summary of the reactions of monomeric electron-rich alkynes with TCNE. The *s-cis* or *s-trans* conformation of the TCBDs is shown according to X-ray crystal structure analysis.

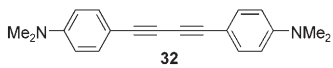
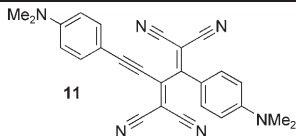
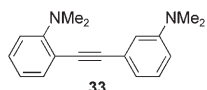
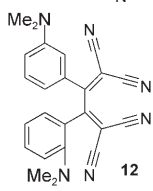
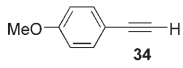
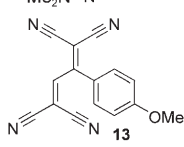
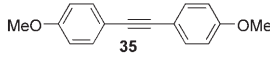
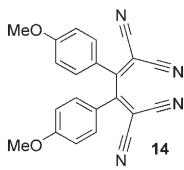
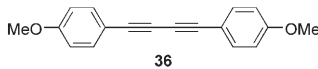
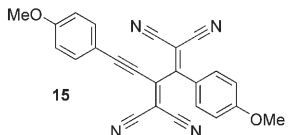
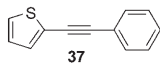
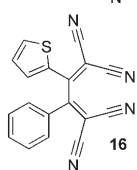
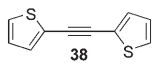
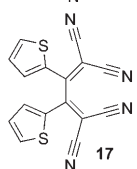
	Alkyne	Product	Yield [%]	Condi- tions
1			97	[a]
2			48	[b]
3			78	[b]
4			27	[c]
5			69	[c]
6			68	[c]
7			8	[b]
8			15	[b]
9			77	[b]
10			100	[d]

Next, we studied the difference in reactivity between the two $\text{C}\equiv\text{C}$ bonds in *p*-DMA-substituted buta-1,3-diyne **28–30** (entries 7–9, Table 1). All butadiynes preferentially reacted with TCNE at the more electron-rich $\text{C}\equiv\text{C}$ bond directly attached to the *p*-DMA donor moiety, resulting in ethynyl-substituted TCBDs. Thus, butadiynes **29** and **30** selectively gave **8** and **9**, respectively, at room temperature. The Me_3Si group of **8** was partially cleaved during column chromatography on SiO_2 , leading to decomposition, whereas the $i\text{Pr}_3\text{Si}$ group of **9** was unaffected. The isolated yields (**8**: 15%; **9**: 77%) clearly reflect this difference in stability between the two silyl protecting groups. On the other hand, only the 4-(dimethylamino)-phenylethynyl-substituted TCBD **7**, resulting from addition to the sterically more accessible terminal $\text{C}\equiv\text{C}$ bond, was isolated in a low yield of 8% from the addition of unprotected **28** to TCNE. We believe, however, that the major product results from addition to the more electron-rich, DMA-substituted $\text{C}\equiv\text{C}$ bond of **28**, leading to Me_3Si -deprotected **8**, which decomposes during chromatographic workup. A second addition to the residual $\text{C}\equiv\text{C}$ bond in **7–9** was not observed, even in the presence of a large excess of TCNE.

Gratifyingly, bis-DMA-substituted alkynes **31–33** provided TCBD molecules **10–12** in almost quantitative yields at room temperature (entries 10–12, Table 1). This result is particularly remarkable for the transformation of **33**, featuring one *o*- and one *m*-DMA moiety.

The comparison between *o*-, *m*-, and *p*-DMA-substituted alkynes (entries 1–6, Table 1) had clearly shown that their reactivity in the cycloaddition with TCNE depends strongly on the electron-donating power of the anilino residue. Correspondingly, alkynes bearing weaker electron-donating substituents, such as *p*-anisyl and 2-thienyl rings, required heating in order to reach a transformation (entries 13–17, Table 1). In particular, the transformations of *p*-anisyl-substituted alkynes were sensitive to the applied temperature. The reaction of **34** in boiling benzene for 5 h afforded the corresponding TCBD **13** in a yield of 32% (entry 13, Table 1), whereas di-*p*-anisyl-substituted alkynes **35** and **36** did not react with TCNE at 80°C. By changing the solvent to boiling toluene

Table 1. (Continued)

	Alkyne	Product	Yield [%]	Condi- tions
11			96	[a]
12			100	[b]
13			32	[c]
14			42	[f]
15			12	[g]
16			80	[h]
17			80	[h]

[a] In C₆H₆, 20 °C, 2–3 h. [b] In CH₂Cl₂, 20 °C, 0.5–1 h. [c] 70 °C, 0.5 h. [d] In THF, 20 °C, 1 h. [e] In C₆H₆, 80 °C, 5 h. [f] In toluene, 110 °C, 12 h. [g] 170 °C, 10 min. [h] 150 °C, 8–14 h.

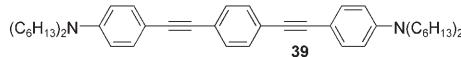
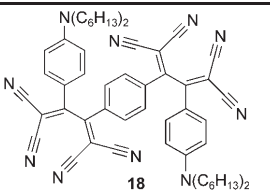
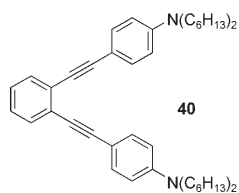
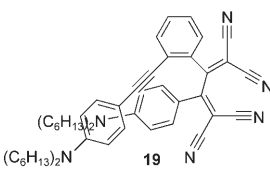
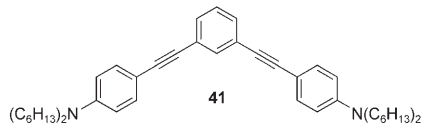
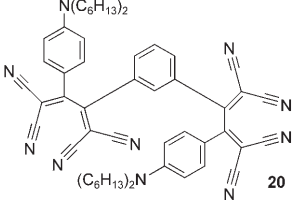
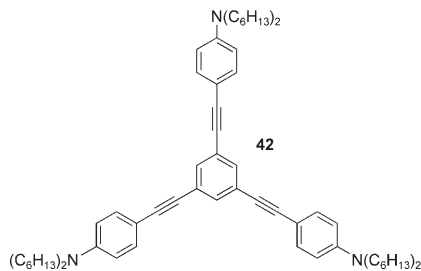
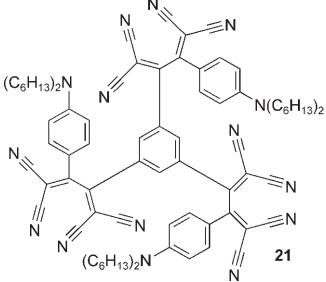
(110 °C), di-*p*-anisyl-substituted TCBD **14** was obtained from **35** in a yield of 42 % (entry 14, Table 1). An even higher temperature was necessary for **36**, and the reaction was very slow below 160 °C, especially in solution, while decomposition of the product dominated above 180 °C. Thus, **15** was obtained in poor yield (12 %) by heating **36** with TCNE in the absence of solvent to 170 °C for only 10 min (entry 15, Table 1). The optimization of the reaction conditions for 2-thienyl-substituted alkynes was facilitated by the higher thermal stability of the products. Thus, 2-thienyl-substituted TCBDs **16** and **17** were obtained in high yield (80 %) from transformations at 150 °C in the absence of solvent (entries 16 and 17, Table 1).

The thermal stability of selected donor-substituted TCBDs was investigated by thermogravimetric analysis (TGA) (see Supporting Information). For some chromophores, decomposition proceeded in two or three steps. The first noticeable decomposition temperatures determined by derivative thermogravimetry ranged from 210 to 450 °C, comparable to those reported for other TCBD derivatives.^[9c] All monomeric TCBDs measured did not show any significant decomposition at least up to the melting points.

Synthesis of oligomeric donor-substituted tetracyanobutadienes: *p*-DMA donors have the highest alkyne-activating power, and TCBDs bearing aryl groups at both 2- and 3-positions are particularly stable. With these results from the preparation of monomeric systems in mind, we targeted novel oligomeric TCBD molecules. To improve the solubility of the molecules, *p*-*N,N*-dihexylanilino (DHA) instead of DMA groups were introduced as donor residues. The DHA-substituted oligoalkyne precursors **39–42**, prepared by Sonogashira cross-coupling of 4-ethynyl-*N,N*-dihexylaniline with di- or trihalobenzenes, immediately reacted with TCNE in CH₂Cl₂ at room temperature, yielding the DHA-substituted TCBDs **18–21** (Table 2). *p*-Phenylene-linked dialkyne **39** furnished the corresponding di-TCBD molecule **18** in a quantitative yield (entry 1, Table 2), whereas *m*-phenylene-linked dialkyne **41** afforded **20** in 86 % yield (entry 3, Table 2). The same yield was obtained in the conversion of **42** to the tri-TCBD derivative **21** with a 1,3,5-trisubstituted benzene core (entry 4, Table 2). The products were stable in the presence of an excess of TCNE and could readily be isolated. The difference in the yields between the *p*- and *m*-phenylene derivatives reflects the differences in the steric accessibility of the alkyne moieties in **39** and **42**. Quadrupolar (e.g., **18**) and octupolar (e.g., **21**) D–A molecules have been shown to feature large two-photon absorption (TPA) cross sections associated with NLO processes.^[11]

In contrast to the *p*- and *m*-phenylene-linked dialkynes, the *o*-phenylene derivative **40** did not produce the expected di-TCBD molecule, but only mono-adduct **19** was isolated in 39 % yield (entry 2, Table 2). In this case, an unidentified side reaction between **19** and TCNE in addition to steric hindrance prevented the cycloaddition of the second alkyne under formation of the targeted di-TCBD molecule.

Table 2. Summary of the reactions of the oligomeric electron-rich alkynes with TCNE.^[a]

	Alkyne	Product	Yield [%]
1			99
2			39
3			86
4			86

[a] In CH₂Cl₂, 20 °C, 3 h.

X-ray structures and bond length alternation: All donor-substituted TCBDs are colored solids. Many of the monomeric chromophores furnished single crystals suitable for X-ray crystallographic analysis by slow diffusion of hexane into a solution of the molecule in CH₂Cl₂ at –15 °C. The crystal structures of **3**, **12**, **13**, **14**, and **17** are shown in Figure 1 (for the crystal structures of **2**, **10**, and **11**, see reference [7] and Supporting Information).

All TCBD moieties are highly distorted. Distortion from planarity occurs mainly by rotation around the central single bond of the TCBD moiety. For example, the twist between the two dicyanovinyl planes in **3** is expressed by the torsion angle $\theta(\text{C}(11)\text{--C}(1)\text{--C}(16)\text{--C}(17)) = 85.5^\circ$. If the absolute value of this torsion angle is less than 90°, the TCBD adopts the *s-cis* conformation. This is the case for compounds **3**, **10**, **12**, **14**, and **17** (Table 3). In contrast, if the absolute value is larger than 90°, the *s-trans* conformation is preferred in the solid state, and this geometry is seen in the crystal structures of compounds **2**, **11**, and **13**. Thus, TCBD derivatives substituted with aryl groups at both 2- and 3-positions prefer the *s-cis* conformation, presumably due to additional favorable intramolecular aryl–aryl interactions.^[12] The angle between

the planes of the dicyanovinyl moieties and the directly attached donor rings vary between $\approx 1^\circ$ (**11**, see Supporting Information) and $\approx 44^\circ$ (**13**, Figure 1). Despite these distortions, nearly all donor-substituted TCBDs undergo efficient intramolecular CT interactions (vide infra).

The crystal packings show several interesting short intermolecular contacts (Figure 2). For example, the DMA residues of two neighboring molecules in the crystal of **3** undergo antiparallel stacking at intermolecular C···C distances around 3.80 Å (Figure 2a). More interesting are the intermolecular interactions of the strong CN dipoles.^[13] A favorable antiparallel dipolar alignment of two CN moieties is observed in the crystal structures of **12** ($d(\text{C}\cdots\text{N}) = 3.28 \text{ Å}$) and **17** ($d(\text{C}\cdots\text{N}) = 3.21 \text{ Å}$), shown in Figure 2b and e, respectively. Additionally, the crystal packing of **17** features two nearly orthogonal, symmetry related CN···CN interactions with a sub van der Waals distance ($d(\text{N}(17')\cdots\text{C}(21'')) = 3.15 \text{ Å}$, $\text{N}\cdots\text{C}\equiv\text{N}$ angle = 95°).

Interestingly, previously unknown nearly orthogonal multipolar contacts are observed in the crystal packings of **13**, **14**, and **17**. The CN groups of one molecule interact with the C(CN)₂ moieties of its neighbor. In **13** (Figure 2c) the shortest contact is observed between N18 and the central vinylic C atom C16' ($d(\text{N}\cdots\text{C}) = 3.17 \text{ Å}$, $\text{N}\cdots\text{C}=\text{C}$ angle = 103°). It is unclear at present whether this contact is favorable or not. However, in this specific alignment, the CN group can form two rather than only one (nearly orthogonal) CN···CN contact ($d(\text{N}(18)\cdots\text{C}(17')) = 3.24 \text{ Å}$, $\text{N}\cdots\text{C}\equiv\text{N}$ angle = 107° and $d(\text{N}(18)\cdots\text{C}(19'')) = 3.41 \text{ Å}$, $\text{N}\cdots\text{C}\equiv\text{N}$ angle = 68°). In the crystal packing of **14**, two neighboring molecules feature two symmetry-related $\text{C}\equiv\text{N}\cdots\text{C}(\text{CN})_2$ interactions, with the N atom pointing in both cases in a near orthogonal fashion onto the three C atoms of the dicyanomethylene fragment (Figure 2d). Two similar $\text{C}\equiv\text{N}\cdots\text{C}(\text{CN})_2$ contacts are seen in the crystal packing of **17** (Figure 2e). Thus, the crystal structures of donor-substituted TCBDs visualize once more the important role of multipolar interactions, and in particular orthogonal ones, in stabilizing organic crystal lattices. A better understanding of such interactions is only just now emerging as an important target of computational and experimental work.^[13]

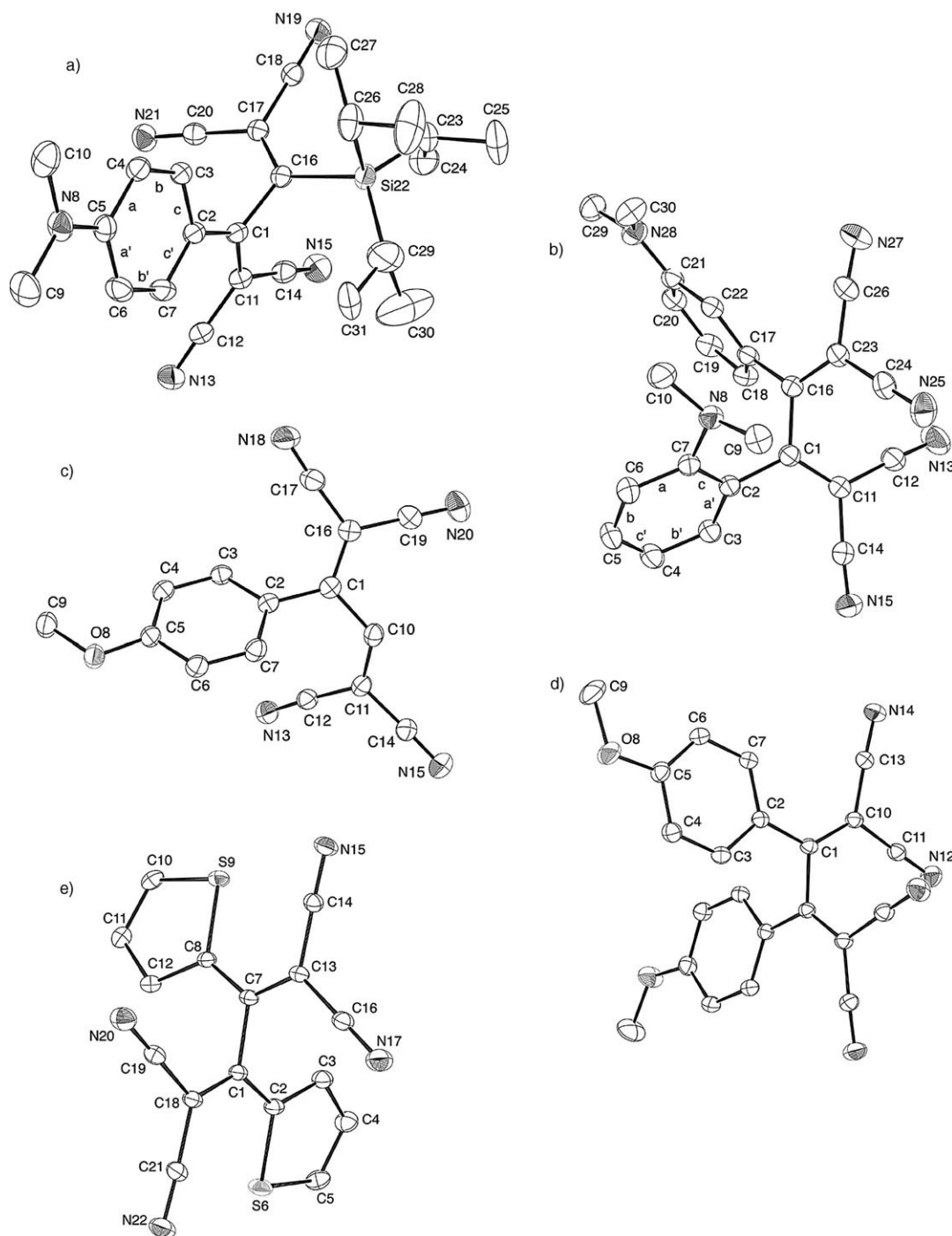


Figure 1. ORTEP plots of a) **3**, b) **12**, c) **13**, d) **14**, and e) **17** with vibrational ellipsoids shown at the 30% probability level. Arbitrary numbering. Selected bond lengths (Å) and angles (°): **3**: C1–C11 1.374(5), C1–C2 1.445(4), C1–C16 1.505(4), C2–C7 1.407(4), C2–C3 1.411(5), C3–C4 1.362(5), C4–C5 1.420(5), C5–N8 1.351(4), C5–C6 1.413(5), C6–C7 1.374(5), C16–C17 1.348(4), C16–Si22 1.948(3); C11–C1–C16 115.0(3), C12–C11–C14 112.6(3), C17–C16–C1 115.3(3), C17–C16–Si22 126.6(2), C18–C17–C20 114.1(3); **12**: C1–C11 1.356(2), C1–C2 1.477(2), C1–C16 1.4942(19), C2–C3 1.402(2), C2–C7 1.404(2), C3–C4 1.377(2), C4–C5 1.375(3), C5–C6 1.381(3), C6–C7 1.402(2), C7–N8 1.409(2); C11–C1–C2 122.21(13), C1–C11–C12 124.05(14), C23–C16–C17 122.29(13), C16–C23–C24 122.81(14); **13**: C1–C16 1.356(4), C1–C2 1.466(3), C1–C10 1.468(4), C2–C3 1.395(4), C2–C7 1.407(3), C3–C4 1.384(4), C4–C5 1.391(4), C5–O8 1.360(3), C5–C6 1.387(4), C6–C7 1.369(4), C10–C11 1.340(4); C2–C1–C10 118.9(2), C11–C10–C1 124.7(2), C12–C11–C14 114.7(2), C19–C16–C17 115.1(2); **14** for one of the two different molecules in the unit cell: C1–C10 1.3658(16), C1–C2 1.4653(16), C2–C7 1.4016(16), C2–C3 1.4102(16), C3–C4 1.3722(17), C4–C5 1.3974(18), C5–O8 1.3500(16), C5–C6 1.3866(19), C6–C7 1.3831(18); C10–C1–C2 127.82(10), C1–C10–C11 121.03(11); **17**: C1–C18 1.3675(19), C1–C2 1.4395(19), C1–C7 1.5121(16), C2–C3 1.4014(19), C2–S6 1.7330(13), C3–C4 1.407(2), C4–C5 1.364(2), C5–S6 1.6951(16); C18–C1–C2 127.45(12), C19–C18–C21 115.77(12). Selected torsion angles (°): **3**: C11–C1–C2–C7 = 19.5(5); **12**: C11–C1–C2–C3 = –41.0(2); C23–C16–C17–C22 = –55.5(2); **13**: C16–C1–C2–C3 = 44.1(4); **14**: C10–C1–C2–C7 = 11.47(19); **17**: C13–C7–C8–S9 = 9.9(2).

Table 3. Correlation of the quinoid character of donor-substituted TCBDs with spectral properties to estimate the efficiency of intermolecular D–A π -conjugation.

	δr [Å]	θ [°] ^[a]	δ_{meta} [ppm] ^[b]	$\nu(\text{C}\equiv\text{N})$ [cm ^{−1}]
2	0.036	−144.3 146.5	7.51	2212
3	0.045	85.5	7.53	2212
10	0.050	62.3	7.79	2206
11	^[c]	−96.7	7.48 7.82	2217
12	0.034 ^[d]	−53.9		2223
13	0.019	−144.5	7.45	2224
14	0.020	75.1 −121.9	7.77	2224
17		88.5		2224

[a] The torsion angle between the two dicyanovinyl planes in the TCBD moieties. [b] ¹H NMR chemical shifts (300 MHz) in CDCl₃. [c] The data are not reliable, see reference [7]. [d] Determined from the *o*-DMA ring.

Bond length alternation in the benzene rings of the DMA and anisyl moieties is a good indication for the efficiency of

the CT conjugation from the donor to the TCBD acceptor moieties, and can be expressed by the quinoid character (δr) of the ring [Eq. (1)].^[14]

$$\delta r = \{[(a + a') - (b + b')]/2 + [(c + c') - (b + b')]/2\}/2 \quad (1)$$

In benzene, the δr value equals 0, whereas values between 0.08 and 0.10 are found in fully quinoid rings (see Figure 1a,b for the definition of bonds *a*, *a'*, *b*, *b'*, *c*, and *c'*). Calculated from the X-ray crystal structures (Figure 1 and reference [7]), TCBD **2** with two different molecules in the unit cell exhibits an average δr of 0.036 (Table 3). TCBDs **3** and **10** show higher values of 0.045 and 0.050, respectively. As a comparison, the δr values for *p*-DMA rings in D–A substituted TEEs, calculated from several X-ray structures, generally do not exceed 0.025.^[2c] Recently reported DMA-substituted CEEs, which were proven to have stronger D–A interactions, display δr values of 0.033–0.037.^[15] Taking into account these results, DMA-substituted TCBDs clearly feature efficient intramolecular CT interactions. Even **12**, with a

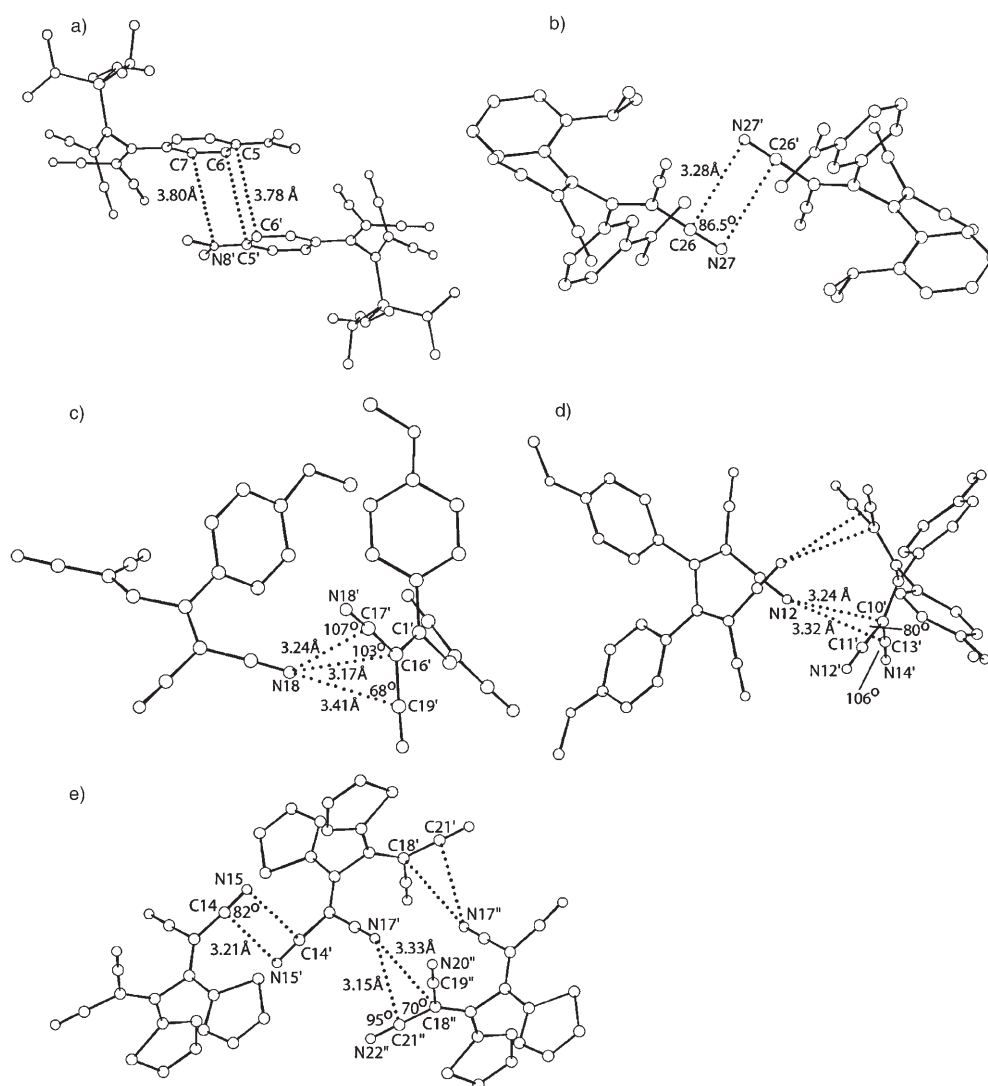


Figure 2. Arrangement of neighboring molecules in the crystal packings of a) **3**, b) **12**, c) **13**, d) **14**, and e) **17**.

substantial twist between the donor and acceptor moieties (see legend to Figure 1), has a value of 0.034 calculated from the *o*-DMA ring. *p*-Anisyl-substituted TCBD derivatives **13** and **14** exhibit reasonably decreased δr values of 0.019 and 0.020, respectively, due to the weaker electron-donating power.

The δr values for *p*-DMA and *p*-anisyl rings display a good correlation with the chemical shifts of the protons in *meta* positions relative to the dimethylamino and methoxy substituents (Table 3). Downfield shifts of the *meta*-protons are measured as a result of the CT from the donor to the acceptor moiety and can be considered as another measure for the efficiency of ground-state D–A conjugation.^[4b] The downfield shifts (and correspondingly the CT efficiency) decrease from **10**, to **3**, and to **2** for *p*-DMA rings and from **14** to **13** for *p*-anisyl rings. This order is consistent with that of the δr values. Note that the downfield shifts resulting from intermolecular CT in **10** and **14** might have been slightly overestimated because of anisotropic through-space effects of the aryl rings, resulting from the *s-cis* orientation of the TCBD moieties.

The vibrational frequency $\nu(\text{C}\equiv\text{N})$ of the TCBD moieties is also correlated with the δr values (Table 3). The shift of this frequency to lower energy can be considered as a good indication for the CT from donor to acceptor moieties. The value of the $\nu(\text{C}\equiv\text{N})$ stretching frequency indeed shifts to low energy as the δr values increase. Taking together into account the X-ray, NMR, and IR data, the efficiency of the CT in the ground state increases in the series **13** < **14** < **12** < **2** < **3** < **10**.

Electrochemistry: The redox properties of the donor-substituted TCBDs were studied using cyclic voltammetry (CV) and rotating disk voltammetry (RDV) in CH_2Cl_2 with $n\text{Bu}_4\text{NPF}_6$ (0.1 M) as the supporting electrolyte. The redox potentials vs. Fc^+/Fc (ferricinium/ferrocene couple) are listed in Table 4.

All monomeric TCBDs show two reversible, well-resolved 1e^- reduction steps centered on the two dicyanovinyl units. Each *p*-DMA moiety undergoes a reversible 1e^- oxidation step, whereas oxidations of *p*-anisyl and 2-thienyl moieties are not observed within the available potential range. The *o*- and *m*-DMA groups of **12** give irreversible oxidations

Table 4. Electrochemistry data of donor-substituted TCBDs in CH_2Cl_2 (+ 0.1 M $n\text{Bu}_4\text{NPF}_6$).^[a] For an overview of the compounds, see Tables 1 and 2.

	Cyclic Voltammetry			Rotating Disk Voltammetry	
	E° [V] ^[b]	ΔE_p [mV] ^[c]	E_p [V] ^[d]	$E_{1/2}$ [V] ^[e]	Slope [mV] ^[f]
2	+0.86	80		+0.87 (1e^-)	70
	−0.69	80		−0.70 (1e^-)	70
	−1.26	90		−1.38 (1e^-)	140
3	+0.90	70		+0.92 (1e^-)	70
	−1.10	90		−1.14 (1e^-)	75
	−1.34	100		[g]	
6	+0.97	90		+1.02 (1e^-)	90
	−1.11	80		−1.14 (1e^-)	75
			−1.74 ^[h]	−1.79 (1e^-) ^[h]	100

Table 4. (Continued)

	Cyclic Voltammetry			Rotating Disk Voltammetry	
	E° [V] ^[b]	ΔE_p [mV] ^[c]	E_p [V] ^[d]	$E_{1/2}$ [V] ^[e]	Slope [mV] ^[f]
7	+0.74	90		[i]	
	−0.55	90		−0.56 (1e^-)	75
	−1.14	90		[j]	
8	+0.91	100		[g]	
	−0.75	110		−0.75 (1e^-)	90
	−1.13	120		−1.20 (1e^-)	[j]
9	+0.90	100		[g]	
	−0.70	75			
	−1.07	100			
10	+0.91	100 ^[k]		+0.89 (2e^-)	125
	+0.86	90			
	−1.06	90		−1.08 (1e^-)	75
11	−1.29	90		−1.36 (1e^-)	100
	+0.90	100		[g]	
	+0.72	90		+0.76 (1e^-)	75
12	−0.89	90		−0.91 (1e^-)	80
	−1.18	90		−1.26 (1e^-)	90
			+1.06 +0.78	[i]	
13	−0.80	120		+0.82 (1e^-)	85
	−1.27	130		−0.88 (1e^-)	80
				−1.41 (1e^-)	100
14	−0.56	90		−0.60 (1e^-)	70
	−1.21	90		−1.30 (1e^-)	80
	−0.81	90		−0.85 (1e^-)	65
15	−1.18	90		−1.25 (1e^-)	65
	−0.65	80		−0.69 (1e^-)	75
	−1.05	80		−1.13 (1e^-)	70
16	−0.75	125		−0.82 (1e^-)	110
	−1.09	125		−1.26 (1e^-)	110
	−0.79	125		−0.85 (1e^-)	110
17	−1.05	115		−1.23 (1e^-)	110
	+0.89	75		+0.91 (2e^-)	60
	−0.75	70		−0.75 (1e^-)	60
18	−0.94	80		−0.97 (1e^-)	65
	−1.26	75		−1.45 (2e^-)	125
	−1.39	80			
19	+0.75	100		+0.87 (1e^-)	75
	+0.52	85		+0.58 (1e^-)	70
	−0.87	85		−0.93 (1e^-)	80
20	−1.10	85		−1.21 (1e^-)	75
	+0.88	60		+0.91 (2e^-)	50
	−0.80	70		−0.82 (1e^-)	60
21	−1.00	80		−1.05 (1e^-)	70
	−1.26	60		−1.50 (2e^-)	100
	−1.39	65			
22	+0.89	80		+0.92 (3e^-)	40
	−0.69	70		−0.73 (1e^-)	65
	−0.82	90		−0.94 (1e^-)	75
23	−1.06	120		−1.15 (1e^-)	[g]
	−1.27	60		−1.35	[g]
	−1.44	70		−1.51	[g]
24	−1.69	60		≈ −1.7	[g]

[a] Potentials versus the ferricinium/ferrocene couple. Working electrode: glassy carbon electrode; counter electrode: Pt; reference electrode: Ag/AgCl . [b] $E^\circ = (E_{\text{pc}} + E_{\text{pa}})/2$, in which E_{pc} and E_{pa} correspond to the cathodic and anodic peak potentials, respectively. All reductions are 1e^- transfers. [c] $\Delta E_p = E_{\text{ox}} - E_{\text{red}}$, in which the subscripts ox and red refer to the conjugated oxidation and reduction steps, respectively. [d] E_p = Irreversible peak potential at sweep rate $\nu = 0.1\text{ V s}^{-1}$. [e] $E_{1/2}$ = Half-wave potential. [f] Slope = Slope of the linearized plot of E versus $\log [I/(I_{\text{lim}} - I)]$. I_{lim} is the limiting current and I the current. [g] Unresolved waves. [h] Small amplitude signal. [i] Electrode inhibition during oxidation. No plateau-limiting current could be observed. [j] Spread-out wave due to surface phenomena (insulating film formation). [k] Could not be determined due to the presence of a cathodic redissolution peak at scan rates lower than 1 V s^{-1} .

due to the absence of substituents in *para* position to the dimethylamino functions: dimerization via the electrogenerated radical cations has been shown to usually occur at such positions.^[16]

Whereas **2** and **3** do not differ much in the first oxidation potential (+0.86 vs +0.90 V), the introduction of the additional *i*Pr₃Si substituent in **3** causes a dramatic cathodic shift of the first reduction potential by 410 mV (−0.69 (**2**) vs −1.10 V (**3**)). On the other hand, compounds **8** and **9**, with Me₃SiC≡C– and *i*Pr₃SiC≡C– substituents, respectively, exhibit only a slight cathodic shift by 60 mV (**8**) and 10 mV (**9**) in their respective first reduction potentials as compared to **2**. These cathodic shifts are a consequence of the greater twist and the resulting enforced deconjugation between the two dicyanovinyl residues of the TCBD moieties upon introduction of the second substituent. These steric effects are evidently larger when the bulky silyl substituent is directly attached to the TCBD skeleton. The X-ray crystal structures of **2** and **3** nicely support this explanation (Table 3, Figure 1); the TCBD chromophore in **2** is more planar than in **3**.

The presence of a second DMA donor also brings about a remarkable cathodic shift of the first reduction potentials. From **10** (two *p*-DMA), to **11** (two *p*-DMA), and to **12** (one *o*-, one *m*-DMA) the observed shifts are −370 mV, −200 mV, and −110 mV, respectively, relative to the first reduction potential of **2** ($E_{\text{red},1} = -0.69$ V). The same tendency, with less pronounced differences in the cathodic shifts, is observed for *p*-anisyl- or 2-thienyl-donor-substituted TCBDs. The values shift by −250 mV and −90 mV for **14** and **15**, respectively, relative to the first reduction potential of *p*-anisyl-substituted TCBD **13** ($E_{\text{red},1} = -0.56$ V). The potential of **17** shifts cathodically by only 40 mV relative to that of thienyl-substituted **16** ($E_{\text{red},1} = -0.75$ V).

Some of these measured potential shifts result from differences in the twist between the two dicyanovinyl residues of the TCBD acceptor as well as from sterically enforced deviations from planarity of individual donor-substituted dicyanovinyl moieties, thereby reducing the extension of π conjugation. But another significant part of the observed shifts is a direct consequence of the extent of D–A coupling.^[4b,17] In a π -conjugated system, the presence of an electron-donating group hinders the electron reduction and an electron-withdrawing group makes the oxidation more difficult. In other words, efficient D–A conjugation leads to a lowering and an elevation of the HOMO and LUMO levels, respectively, and weaker D–A coupling, in contrast, brings about an elevation and a lowering of the HOMO and LUMO levels, respectively. As an example, the structure of TCBD **7** is an expanded version of **2**, with an ethynediyl spacer inserted between the DMA donor and the TCBD acceptor. The first reduction potential of **7** is anodically shifted by 140 mV relative to that of **2**, and the first oxidation potential is, in contrast, cathodically shifted by 120 mV. Thus, the electrochemical HOMO–LUMO gap of **7** (1.29 eV) is much smaller than that of **2** (1.55 eV). The value of 1.29 V is the lowest in the entire series. This result clearly shows that there is much

less efficient coupling between the DMA donor and the TCBD acceptor in **7** because of the ethynediyl spacer.

Interestingly, the comparison of the CV data of *p*-DMA- and *p*-anisyl-substituted TCBDs allows the extrapolation of the yet unknown first reduction potential of the unsubstituted TCBD chromophore. Plotting the first reduction potentials as a function of the number of the donor substituents (*n*) affords two lines with different slopes (Figure 3). Defini-

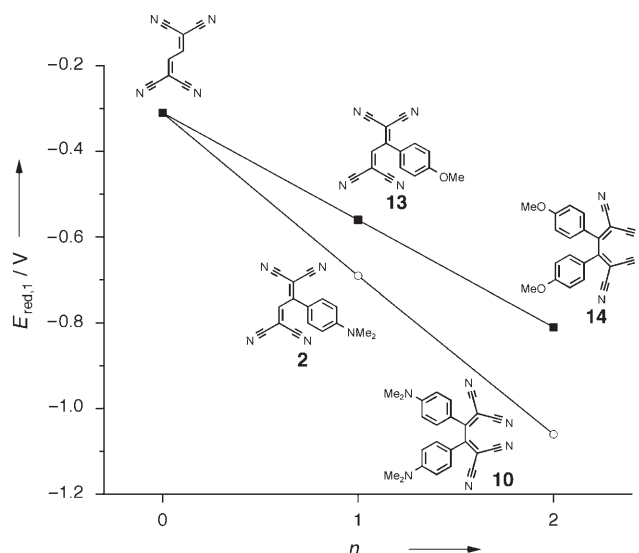


Figure 3. Linear correlation between the number of donor substituents (*n*) on the TCBD moiety and the first reduction potential $E_{\text{red},1}$. ○: *p*-DMA donors, ■: *p*-anisyl donors.

tively, the *p*-DMA moiety is a more powerful electron-donating group than the *p*-anisyl moiety, shifting the first reduction potential to more negative potentials by 130 mV (**2** against **13**; one donor group) and 250 mV (**10** against **14**; two donor groups). The latter value is about twice as large as the former one, which is a good indication of the additivity of the substituent effects (Hammett correlation)^[18] on the TCBD chromophore. This additivity is the overlap of both the electronic effect and the enforced deconjugation of the TCBD moiety, sterically induced by the second donor group. The two lines are crossing each other at *n*=0, indicating that the unsubstituted TCBD will probably be reduced at -0.31 ± 0.01 V. This value is comparable to that of TCNE (−0.32 V).^[19]

The dimeric TCBD derivatives **18** and **20** exhibit four TCBD-centered reduction steps and one DMA-centered oxidation wave. The first two 1e[−] reduction potentials reflect the difference in the connector (*p*- or *m*-phenylene) between the two TCBD moieties. The oxidation peak shape is indicative of two overlapping one-electron transfers, which means that the two DMA groups are far away from each other, avoiding any electrostatic repulsion between the oxidized sites. RDV confirmed the exchange of two electrons for the oxidative process by comparing the wave amplitudes of the oxidation and reduction processes. Whereas the first two re-

ductions are well resolved, the third and fourth reductions give rise to a unique spread-out wave, due to the formation of insulating films with potentials more negative than those observed by CV (for CV traces, see Supporting Information).

TCBD **19** shows reversible electron transfers, namely two oxidation and two reduction steps. The first reduction potential is attributed to the TCBD moiety. The first oxidation potential is derived from the ethynylated DMA moiety, because the other DMA moiety, which is directly attached to the TCBD acceptor, is more difficult to oxidize. Thus, the interaction between HOMO and LUMO levels is weak, leading to the low electrochemical HOMO–LUMO gap of 1.39 V.

Remarkably, one large oxidation peak and six reversible reduction steps are detected in the CV of the trimeric TCBD molecule **21** (Supporting Information). The limiting current for the six reduction steps observed by RDV at -1.8 V is twice as large as the limiting oxidation current. Since the oxidation involves three-electron transfers derived from three DMA groups, it is reasonable to conclude that each reduction step occurs as a $1e^-$ transfer. A conjugated organic molecule that shows six successive and reversible $1e^-$ reduction steps within a narrow potential range of 1.0 V (from -0.69 V to -1.69 V in this case) is, to our knowledge, unprecedented. Careful examination of the oxidation wave shape provided the wave slope of 40 mV, indicating that structural change might have occurred after the first oxidation.^[20]

UV-visible spectroscopy: Most of the donor-substituted TCBDs show multiple CT bands, resulting from different D–A transitions. For example, **2** displays two rather weak CT bands at 481 and 570 nm (2.58 and 2.18 eV, respectively; Figure 4). These bands are derived from two different D–A transitions, involving different donor-located orbitals (vide infra). The weaker D–A interaction reasonably shifts the CT band to lower energy. Substitution of **2** with the iPr_3Si

group results in a hypsochromic shift of the longest wavelength absorption maximum of **3** (λ_{max} : 454 nm (2.73 eV)), reflecting sterically enforced deconjugation. This deconjugation of the TCBD moiety elevates the LUMO level, thereby resulting in a larger band gap. The spectra of **8** and **9** feature a distinct band at nearly the same energy as **3**, with an additional broad shoulder at about 550 nm (2.25 eV). In contrast, the CT band of the expanded TCBD **7** is composed of a single, rather intense absorption, significantly shifted to lower energy (698 nm (1.78 eV), Table 5). The single CT

Table 5. Summary of the UV-visible spectra of donor-substituted TCBDs in CH_2Cl_2 and electrochemical band gaps determined by CV in CH_2Cl_2 .^[a]

	λ_{max} [nm (eV)]	λ_{end} [nm (eV)]	$\Delta(E_{ox,1}-E_{red,1})$ [V]
2	570 (2.18)	960 (1.29)	1.55
3	454 (2.73)	630 (1.97)	2.00
7	698 (1.78)	990 (1.25)	1.29
8	^[b]	760 (1.63)	1.66
9	550 ^[c] (2.25)	790 (1.57)	1.60
10	470 (2.64)	660 (1.88)	1.92
11	526 (2.36)	780 (1.59)	1.61
18	^[b]	810 (1.53)	1.64
19	^[b]	980 (1.27)	1.39
20	^[b]	765 (1.62)	1.68
21	590 ^[c] (2.10)	800 (1.55)	1.58

[a] The optical band gap is either determined from λ_{max} of the CT band or from the optical end-absorption λ_{end} . [b] Could not be determined due to strong peak broadening. [c] Shoulder.

band indicates that the DMA donor in **7** senses the TCBD moiety as a single acceptor in **7**, presumably due to the absence of a substantial twist between the two dicyanovinyl moieties. The lower energy of the CT band of **7**, relative to that found for **2**, clearly reflects the weaker D–A coupling as a result of the insertion of the ethynediyl spacer (vide supra). As previously observed in the study of donor-substituted CEEs,^[4b] the acetylenic spacer serves as an “insulator” between donor and acceptor moieties and this decoupling leads to a decrease in both optical and electrochemical HOMO–LUMO gaps.

Introduction of a second *p*-DMA donor group dramatically increases the intensity of the CT bands (Figure 5). The longest wavelength CT bands of **10** and **11** feature a λ_{max} of 470 nm (2.64 eV) with a molar extinction coefficient (ϵ) of $55000\text{ M}^{-1}\text{ cm}^{-1}$ and a λ_{max} of 526 nm (2.36 eV) with ϵ of $38100\text{ M}^{-1}\text{ cm}^{-1}$, respectively. In contrast, **12** with *o*- and *m*-DMA donors exhibits a much weaker, nearly vanishing CT absorption. Upon protonation of the DMA moieties with trifluoroacetic acid (TFA), the solutions of **10** and **11** turn from purple to colorless and the longest wavelength absorption bands disappear almost completely. The CT bands can be fully regenerated upon neutralization with Et_3N .

The spectral behavior of the *p*-anisyl donor-substituted TCBDs **13–15** is similar to that of the corresponding *p*-DMA-substituted analogues **2**, **10**, and **11** (Supporting Information). Di-*p*-anisyl-substituted TCBDs **14** and **15** exhibit more intense CT bands than **13**, and their absorption maxima are hypsochromically shifted relative to that of **13**

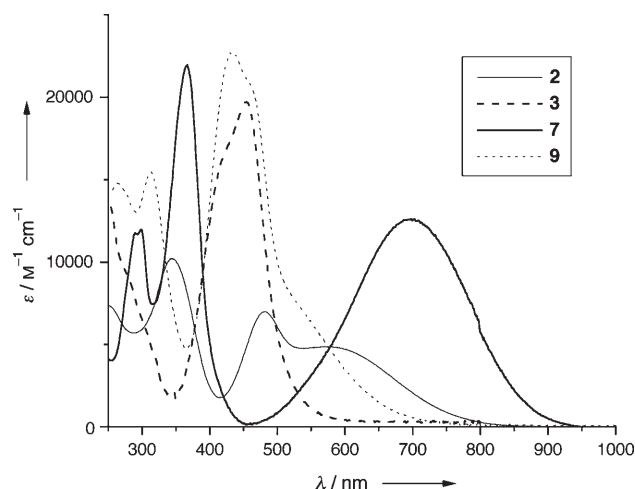


Figure 4. UV-visible spectra of monomeric DMA donor-substituted TCBDs in CH_2Cl_2 .

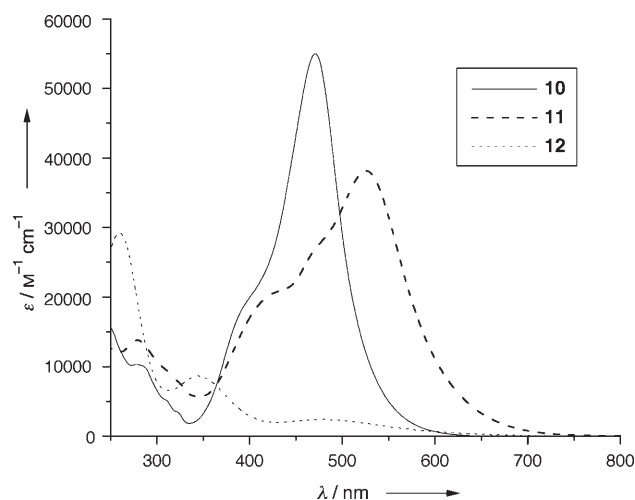


Figure 5. UV-visible spectra of bis-DMA donor-substituted TCBDs in CH_2Cl_2 .

by 66 nm (0.48 eV) and 21 nm (0.14 eV), respectively. Di-thienyl-substituted TCBD **17** displays a λ_{max} of 366 nm (3.39 eV) with double the intensity of **16** (369 nm (3.36 eV)), again resulting from the double number of donor substituents.

The CT bands of oligomeric TCBDs feature very large ϵ values and are accompanied with a long tail or shoulder reaching into the near infrared (Supporting Information, Table 5). Thus, the spectrum of dimeric **18** displays a CT band with a λ_{max} of 476 nm (2.61 eV) and ϵ of $99\,900\text{ M}^{-1}\text{ cm}^{-1}$. This ϵ value is almost twice as large as that of *m*-phenylene-linked analogue **20** ($\epsilon = 54\,200\text{ M}^{-1}\text{ cm}^{-1}$) and exceeds even that of trimeric **21** ($\epsilon = 90\,700\text{ M}^{-1}\text{ cm}^{-1}$). As expected, the CT band of **18**, with a *p*-phenylene connector, is bathochromically shifted from the band in **20**, with a *m*-phenylene connector.

A plot of the optical band gap, calculated from the λ_{max} of the CT band or the end-absorption λ_{end} in the UV-visible/NIR spectrum, against the difference between the first oxidation potential and the first reduction potential in the CV (the electrochemical band gap, Table 5) shows a linear correlation ($R=0.978$ for λ_{max} and $R=0.954$ for λ_{end}) between the two quantities (Figure 6). This suggests that the same orbitals are involved in both optical and electrochemical band gaps.

Some optical band gaps, especially of oligomeric TCBDs, could not be determined from λ_{max} , due to broad and weak lowest energy transitions. Weak D–A interactions usually result in an obscure CT band with a relatively low ϵ .^[4b] However, most of these D–A molecules are gratifyingly redox active species, yielding the electrochemical band gaps. By applying the electrochemical band gaps to the correlation, the optical band gaps from λ_{max} were estimated to be 546 nm (2.27 eV, **18**), 636 nm (1.95 eV, **19**), and 532 nm (2.33 eV, **20**). These values are reasonably located on the broad CT bands. This result suggests that the electrochemi-

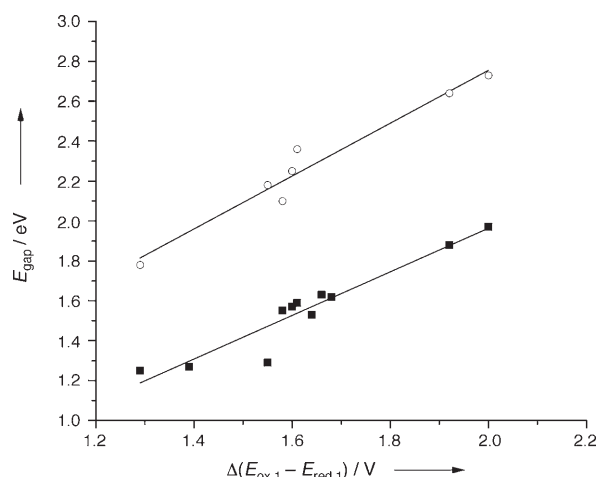


Figure 6. Linear correlation between the optical band gap E_{gap} , determined from λ_{max} (○) for **2**, **3**, **7**, **9**, **10**, **11**, and **21** and λ_{end} (■) for **2**, **3**, **7**, **8**, **9**, **10**, **11**, **18**, **19**, **20**, and **21**, and $\Delta(E_{\text{ox},1} - E_{\text{red},1})$.

cal data can also be used to predict the CT band for weakly coupled D–A interactions.

Fluorescence and solvatochromism: Donor-substituted TCBD molecules do not fluoresce in CHCl_3 , but some of them show a very weak emission in hexane (see Supporting Information). The highest quantum yield determined is 0.015 for **16**. However, some species show very large Stokes shifts of $\sim 7000\text{ cm}^{-1}$, indicating a large transition dipole moment.

A distinct solvatochromism is observed for all donor-substituted TCBDs in various hexane/ CHCl_3 mixtures (see Supporting Information). Noncentrosymmetric bis-DMA-substituted TCBD **11** exhibits the largest solvent effect. From CHCl_3 ($\lambda_{\text{max}} = 526\text{ nm}$, 2.36 eV) to hexane ($\lambda_{\text{max}} = 477\text{ nm}$, 2.60 eV), a shift of 0.24 eV is observed. It is generally known that solvatochromism is a characteristic behavior of dipolar molecules.^[21] However, centrosymmetric molecules such as **10**, **14**, **17**, and **18** as well as the octupolar-type molecule **21** also display solvatochromic effects similar to those measured for the noncentrosymmetric dipolar donor-substituted TCBDs. As an example, the absorption maximum of **14** shifts from 379 nm (3.27 eV) in CHCl_3 to 358 nm (3.46 eV) in hexane. A strong CT from the ground to the excited state would produce a partially positive charge on the donors and a negative charge on the acceptors, which forms a quadrupole for **10**, **14**, **17**, and **18** and an octupole for **21**. We therefore propose that the increase in electric moment from the ground to the excited state through a change in the quadrupole or octupole moment is the most likely explanation for the solvatochromic effects observed for these molecules.^[4b,22]

Computational studies: We recently performed B3LYP/6-31G** calculations^[23] using the Gaussian 98 program^[24] on donor-substituted CEEs, such as **1**, and found good correlations of the results of geometry optimizations with the ex-

perimental data from X-ray crystal structures.^[15] These results were nicely reproduced in the present study in which the B3LYP/6–31G** method implemented in Spartan'04^[25] was used. Geometry optimizations were subsequently performed on TCBDs **2** and **10**, producing good agreement with the X-ray structure data (see Supporting Information). Thus, calculated and experimental bond lengths and torsion angles were in good agreement except for the calculated torsion angle (78.81°) about the central single bond in the TCBD moiety of **10**, which deviated by more than 15° from the experimental value (62.29°). The experimental torsion angle seems to be influenced by crystal packing forces, which are absent in theoretical (gas-phase) geometry determination. For **2**, the calculated quinoid character ($\delta r = 0.035$) was in good agreement with the experimental value (0.036, Table 3), whereas a substantial deviation between experimental (0.050) and calculated value (0.036) was found for **10**.

The HOMOs and LUMOs resulting from the calculations are depicted in Figure 7. For both **2** and **10**, the density in

Table 6. Experimental electronic transitions for TCBDs **2** and **10**, derived from the UV-visible spectra in CH₂Cl₂, and computed values, based on the TD-B3LYP/6–31G**/B3LYP/6–31G* method.^[a]

	Experimental		Computed Values		Composition of band/ CI coefficients	
	λ [nm]	ϵ [M ⁻¹ cm ⁻¹]	λ [nm]	f		
2	343	10200	347	0.29	H–3→L	0.11
					H–2→L	0.11
					H–1→L	0.57
					H→L+1	0.22
	481	7000	403	0.0005	H–2→L	0.69
					H–1→L	–0.14
10	570	4900	659	0.13	H→L	0.64
					H→L+1	–0.11
	390	17900 ^[b]	384	0.58	H–1→L	–0.27
					H→L+1	0.57
	470	55000	457	0.03	H–1→L	0.6
					H→L+1	0.34
			473	0.08	H–1→L+1	0.27
					H→L	0.63

[a] f = oscillator strength; CI = configuration interaction; H = HOMO; L = LUMO. [b] Shoulder.

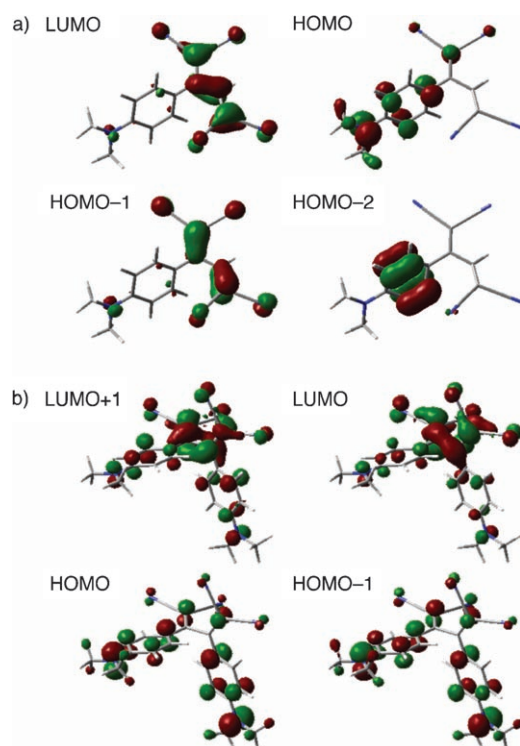


Figure 7. Orbital plots of a) **2** and b) **10**.

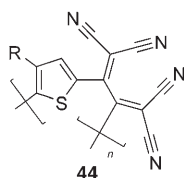
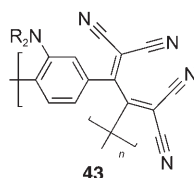
the HOMO is concentrated on the DMA moiety and the density in the LUMO on the TCBD part. The HOMOs show a partial CT from the DMA to the TCBD fragment. Electronic transition analysis for TCBDs **2** and **10** (TD-B3LYP/6–31G**/B3LYP/6–31G*) was performed by using Gaussian 98^[24] (Table 6). The electronic transition analysis of compound **2** suggests that both weak absorption bands result from a D–A transition. The longer wavelength ab-

sorption is mainly a HOMO–LUMO transition (Figure 7), whereas the second band at higher energy is a transition from the DMA-located HOMO–2 to the LUMO level. Similarly, the lowest energy transition of **10** is a HOMO–LUMO transition. Overall, the calculations reproduce well the geometric and electronic properties of TCBDs **2** and **10**.

Conclusion

A series of monomeric, donor-substituted TCBD molecules was synthesized in a remarkable one-step synthesis consisting of the [2+2] cycloaddition between TCNE and electron-rich alkynes, followed by electrocyclic ring opening of the initially formed cyclobutene. Reaction yields are largely dependent on the strength of the donor attached to the alkynes and steric factors. Based on the findings in the synthesis of monomeric TCBDs, oligomeric TCBDs were also prepared in good yields from DMA donor-substituted alkynes attached to *m*- and *p*-phenylene or 1,3,5-benzenetriyl cores. The opportunity for future extension to polymeric structures such as **43** and **44** is indicated by the successful preparation of TCBDs **12** and **17**. Reaction between the corresponding oligo- and poly(arylene ethynylene)s^[26] and an excess of TCNE should yield these novel, alternate D–A polymers. As an advantage, the excess of TCNE will not lead to undesirable side reactions and should be readily removable by vacuum sublimation. These polymers could serve not only as efficient NLO materials, but also as low-band-gap-conjugated polymers, which are interesting because of high intrinsic conductivity in the neutral state and tunable electroactive properties upon doping.^[27]

Despite considerable twists of the two dicyanovinyl moieties around the connecting single bond, as well as deviations of dicyanovinyl moieties and attached donor rings from co-



planarity, donor-substituted TCBDs feature strong intramolecular CT bands in their UV-visible spectra. The efficiency of the intramolecular CT interactions and the D–A coupling is readily deduced from ground-state properties such as bond length alternation determined from the X-ray crystal structures, ^1H NMR chemical shifts, shifts in the frequency of the CN stretching vibration, and electrochemical redox potentials. As discussed previously for donor-substituted CEEs, the position of the longest wavelength CT absorption in the UV-visible spectra is not a good measure for the efficiency of D–A conjugation: stronger D–A coupling leads to higher energy absorptions, whereas weaker coupling between strong donor and acceptor moieties results in lower HOMO–LUMO gaps. The present study confirms that this concept is of general utility to predict the band gap of conjugated D–A molecules.^[28]

Lastly, but not least, the monomeric donor-substituted TCBDs were revealed to be thermally stable up to their high melting points. They are small enough to be sublimed without decomposition under laboratory conditions, which offers the potential for ultra-thin film preparation by vapor deposition techniques.^[29] Applications of this readily available new class of D–A compounds in NLO^[7] and other optoelectronic devices represent a worthwhile objective for future work.

Experimental Section

Materials and general methods: Chemicals were purchased from Acros, Aldrich, and Fluka, and used as received. THF was distilled from Na/benzophenone and $i\text{Pr}_2\text{NH}$ from CaH_2 . Hay catalyst refers to a freshly prepared solution of CuCl (100 mg, 1.0 mmol) and N,N,N',N' -tetramethylethylenediamine (TMEDA; 0.15 mL, 1.0 mmol) in acetone (25 mL). TCNE was purified by sublimation, followed by recrystallization from CH_2Cl_2 . The reactions with TCNE and Pd catalysts were carried out under an inert atmosphere by applying a positive pressure of Ar. Compounds **2**,^[7] **10**,^[7] **11**,^[7] **22**,^[30] **23**,^[31] **26**,^[32] **31**,^[33] **32**,^[32] **35**,^[34] **36**,^[35] **37**,^[36] **38**,^[37] and 4-ethynyl- N,N -dihexylaniline^[38] were prepared according to literature procedures. Column chromatography (CC) and plug filtrations were carried out with Fluka SiO_2 60 (particle size 40–63 μm , 230–400 mesh) or Fluka Al_2O_3 (particle size 50–150 μm) and distilled technical solvents. Size-exclusion chromatography (GPC) was carried out with Bio-beads S-X3 from the company Bio-Rad and distilled technical solvents. Melting points (M.p.) were measured in open capillaries with a Büchi Melting Point B540 apparatus and are uncorrected. “Decomp” refers to decomposition. Some melting/decomposition points could not be determined due to the low stability of the compounds. Thermogravimetric analysis (TGA) was carried out on a Mettler Toledo TGA/SDTA851^o under nitrogen flow, at a heating rate of $10^\circ\text{C min}^{-1}$ between 20°C and 750°C . ^1H NMR and ^{13}C NMR spectra were measured on a Varian Gemini 300 MHz or a Varian Gemini 500 MHz spectrometer at 20°C . Chemical shifts are reported in ppm downfield from SiMe_4 , with the solvent’s residual signal as an internal reference. Coupling constants (J) are

given in Hz. The resonance multiplicity is described as s (singlet), brs (broad singlet), d (doublet), t (triplet), q (quintet), sept (septet), and m (multiplet). Infrared spectra (IR) were recorded on a Perkin–Elmer FT1600 spectrometer. UV-visible spectra were recorded on a Varian CARY-5 spectrophotometer. The spectra were measured in a quartz cuvette of 1 cm. The absorption wavelengths are reported in nm with the extinction coefficient in $\text{M}^{-1}\text{cm}^{-1}$ in brackets. Shoulders are indicated as sh. Fluorescence spectra were measured on a Jobin Yvon Horiba Spex Fluorolog 3 spectrophotometer. Quantum yields were determined versus rhodamine 6G ($\phi_F=0.95$)^[39] or anthracene ($\phi_F=0.32$).^[40] EI-MS and ESI-MS spectra were measured on a Hitachi–Perkin–Elmer VG-TRIBID spectrometer and a Finnigan Mat TSQ 7000 spectrometer, respectively. High-resolution (HR) FT-MALDI spectra were measured on an Ionspec Fourier transform instrument with 2,5-dihydroxybenzoic acid (DHB), *trans*-2-[3-(4-*tert*-butylphenyl)-2-methylprop-2-enylidene]malononitrile (DCTB), or 3-hydroxypicolinic acid (3-HPA) in $\text{MeOH}/\text{H}_2\text{O}$ as matrix, and the compound in CH_2Cl_2 (two-layer technique). The most important signals are reported in m/z units with M as the molecular ion. Elemental analyses were performed by the Mikrolabor at the Laboratorium für Organische Chemie, ETH Zürich.

Electrochemistry: Electrochemistry measurements were carried out at 20°C in CH_2Cl_2 containing 0.1 M $n\text{Bu}_4\text{NPF}_6$ in a classical three-electrode cell. CH_2Cl_2 was purchased in spectroscopic grade from Merck, dried over molecular sieves (4 Å), and stored under Ar prior to use. $n\text{Bu}_4\text{NPF}_6$ was purchased in electrochemical grade from Fluka and used as received. The working electrode was a glassy carbon disk electrode (2 mm in diameter) used either motionless for CV (0.1 to 10 V s^{-1}) or as rotating disk electrode for rotating disk voltammetry (RDV). The auxiliary electrode was a platinum wire, and the reference electrode was an aqueous Ag/AgCl electrode. All potentials are referenced to the ferricinium/ferrocene (Fc^+/Fc) couple, used as an internal standard, and are uncorrected from ohmic drop. The accessible range of potentials on the glassy carbon electrode was $+1.4$ to -2.4 V versus Fc^+/Fc in CH_2Cl_2 . The electrochemical cell was connected to a computerized multipurpose electrochemical device AUTOLAB (Eco Chemie BV, Utrecht, The Netherlands), and controlled by the GPSE software, running on a personal computer.

X-ray analysis: The structures were solved by direct methods (SIR97)^[41] and refined by full-matrix least-squares analysis (SHELXL-97).^[42] using an isotropic extinction correction. All heavy atoms were refined anisotropically; H atoms were refined isotropically, whereby H-positions are based on stereochemical considerations.

X-ray crystal structure of 3: Crystal data at 220(2) K for $\text{C}_{25}\text{H}_{31}\text{N}_5\text{Si}\cdot\text{CH}_2\text{Cl}_2$, $M_r=514.56$, monoclinic, space group $P2_1/n$ (no. 14), $\rho_{\text{calcd}}=1.216\text{ g cm}^{-3}$, $Z=4$, $a=13.2717(4)$, $b=14.2125(4)$, $c=15.8651(5)$ Å, $\beta=110.061(1)^\circ$, $V=2810.98(15)$ Å³; Bruker-Nonius Kappa-CCD diffractometer, $\text{MoK}\alpha$ radiation, $\lambda=0.7107$ Å, $\mu=0.296\text{ mm}^{-1}$. A red crystal of **3** (linear dimensions ca. $0.18\times0.16\times0.13\text{ mm}$) was obtained by slow diffusion of hexane into a solution of compound **3** in CH_2Cl_2 at -15°C . Numbers of measured and unique reflections were 9190 and 4925, respectively ($R_{\text{int}}=0.035$). The $i\text{Pr}_3\text{Si}$ group exhibited static disorder, which was resolved for C23, C25, C26, and C28 (not shown in Figure 1). Final $R(F)=0.082$, $wR(F^2)=0.228$ for 343 parameters and 3689 reflections with $I>2\sigma(I)$ and $2.85<\theta<25.05^\circ$ (corresponding R -values based on all 4925 reflections are 0.105 and 0.253, respectively).

X-ray crystal structure of 12: Crystal data at 223(2) K for $\text{C}_{24}\text{H}_{20}\text{N}_6$, $M_r=392.46$, triclinic, space group $P\bar{1}$ (no. 2), $\rho_{\text{calcd}}=1.214\text{ g cm}^{-3}$, $Z=2$, $a=8.8810(5)$, $b=9.8950(7)$, $c=13.6052(12)$ Å, $\alpha=82.105(4)^\circ$, $\beta=86.857(3)^\circ$, $\gamma=65.047(3)^\circ$, $V=1073.71(14)$ Å³. Bruker-Nonius Kappa-CCD diffractometer, $\text{MoK}\alpha$ radiation, $\lambda=0.7107$ Å, $\mu=0.076\text{ mm}^{-1}$. A black crystal of **12** (linear dimensions ca. $0.26\times0.23\times0.20\text{ mm}$) was obtained by slow diffusion of hexane into a solution of compound **12** in CH_2Cl_2 at -15°C . Numbers of measured and unique reflections were 6809 and 4124, respectively ($R_{\text{int}}=0.022$). Final $R(F)=0.050$, $wR(F^2)=0.121$ for 296 parameters and 3348 reflections with $I>2\sigma(I)$ and $2.53<\theta<26.01^\circ$ (corresponding R values based on all 4124 reflections are 0.064 and 0.130, respectively).

X-ray crystal structure of 13: Crystal data at 223(2) K for $\text{C}_{15}\text{H}_8\text{N}_4\text{O}$, $M_r=260.25$, monoclinic, space group $P2_1/c$ (no. 14), $\rho_{\text{calcd}}=1.316\text{ g cm}^{-3}$, $Z=4$, $a=13.4460(7)$, $b=13.3106(5)$, $c=7.4402(3)$ Å, $\beta=99.396(1)^\circ$, $V=1073.71(14)$ Å³.

1313.74(10) Å³. Bruker-Nonius Kappa-CCD diffractometer, MoK α radiation, λ = 0.7107 Å, μ = 0.088 mm⁻¹. A red crystal of **13** (linear dimensions ca. 0.21 × 0.13 × 0.04 mm) was obtained by slow diffusion of hexane into a solution of compound **13** in CH₂Cl₂ at -15°C. Numbers of measured and unique reflections are 4005 and 2359, respectively (R_{int} = 0.044). Final $R(F)$ = 0.060, $wR(F^2)$ = 0.150 for 191 parameters and 1797 reflections with $I > 2\sigma(I)$ and $3.07 < \theta < 25.40^\circ$ (corresponding R -values based on all 2359 reflections are 0.080 and 0.160, respectively).

X-ray crystal structure of 14: Crystal data at 223(2) K for C₂₂H₁₄N₄O₂, M_r = 366.37, monoclinic, space group $C2/c$ (no. 15), ρ_{calcd} = 1.302 g cm⁻³, Z = 8, a = 14.9643(3), b = 12.8404(3), c = 19.4643(4) Å, β = 92.113(1)°, V = 3737.48(14) Å³. Bruker-Nonius Kappa-CCD diffractometer, MoK α radiation, λ = 0.7107 Å, μ = 0.087 mm⁻¹. A yellow crystal of **14** (linear dimensions ca. 0.21 × 0.18 × 0.17 mm) was obtained by slow diffusion of hexane into a solution of compound **14** in CH₂Cl₂ at -15°C. Numbers of measured and unique reflections are 6835 and 3796, respectively (R_{int} = 0.016). Final $R(F)$ = 0.042, $wR(F^2)$ = 0.112 for 270 parameters and 3259 reflections with $I > 2\sigma(I)$ and $2.09 < \theta < 26.39^\circ$ (corresponding R values based on all 3796 reflections are 0.050 and 0.120, respectively).

X-ray crystal structure of 17: Crystal data at 203(2) K for C₁₆H₆N₄S₂, M_r = 318.37, triclinic, space group $P\bar{1}$ (no. 2), ρ_{calcd} = 1.429 g cm⁻³, Z = 2, a = 8.4001(2), b = 8.5650(2), c = 10.8960(3) Å, α = 81.033(2), β = 81.365(1), γ = 74.127(1)°, V = 740.04(3) Å³. Bruker-Nonius Kappa-CCD diffractometer, MoK α radiation, λ = 0.7107 Å, μ = 0.359 mm⁻¹. A yellow crystal of **17** (linear dimensions ca. 0.25 × 0.23 × 0.19 mm) was obtained by slow diffusion of hexane into a solution of compound **17** in CH₂Cl₂ at -15°C. Numbers of measured and unique reflections are 5773 and 3367, respectively (R_{int} = 0.018). Final $R(F)$ = 0.033, $wR(F^2)$ = 0.094 for 208 parameters and 2996 reflections with $I > 2\sigma(I)$ and $2.54 < \theta < 27.47^\circ$ (corresponding R -values based on all 3367 reflections are 0.038 and 0.098, respectively). CCDC-274233 (**3**), CCDC-274235 (**12**), CCDC-274231 (**13**), CCDC-274232 (**14**), and CCDC-274234 (**17**) contain the supplementary crystallographic data for this paper. These data can be obtained free of charge from The Cambridge Crystallographic Data Centre via www.ccdc.cam.ac.uk/data_request/cif. The crystal structures of **2**, **10**, and **11** are described in reference [7].

2-[4-(Dimethylamino)phenyl]buta-1,3-diene-1,1,4,4-tetracarbonitrile (2): A solution of TCNE (176 mg, 1.37 mmol) in C₆H₆ (15 mL) was added to **22** (200 mg, 1.38 mmol). The mixture was stirred for 2.5 h at 20°C. Evaporation and CC (CH₂Cl₂) afforded **2** (364 mg, 97%) as a purple solid. M.p. 144–145°C; ¹H NMR (300 MHz, CDCl₃): δ = 3.16 (s, 6H), 6.75 (d, J = 9 Hz, 2H), 7.51 (d, J = 9 Hz, 2H), 8.02 ppm (s, 1H); ¹³C NMR (75 MHz, CDCl₃): δ = 40.26, 77.98, 97.19, 109.06, 111.51, 112.10, 113.13, 113.74, 117.66, 132.11, 154.32, 156.67, 158.81 ppm; IR (neat): $\tilde{\nu}$ = 3028, 2921, 2212, 1600, 1486, 1435, 1379, 1346, 1294, 1212, 1172, 942, 821 cm⁻¹; UV/Vis (CH₂Cl₂): λ (ϵ) = 343 (10200), 481 (7000), 570 nm (4900); EI-MS (70 eV): m/z : 273 [M]⁺; elemental analysis calcd (%) for C₁₆H₁₁N₅ (273.29): C 70.32, H 4.06, N 25.63; found: C 70.13, H 4.08, N 25.35.

2-[4-(Dimethylamino)phenyl]-3-(triisopropylsilyl)buta-1,3-diene-1,1,4,4-tetracarbonitrile (3): TCNE (45 mg, 0.35 mmol) was added to a solution of **24** (105 mg, 0.348 mmol) in CH₂Cl₂ (3 mL). The mixture was stirred for 1 h at 20°C. Evaporation and CC (CH₂Cl₂) afforded **3** (117 mg, 78%) as a red solid. M.p. 175–177°C; ¹H NMR (300 MHz, CDCl₃): δ = 1.10 (d, J = 7 Hz, 9H), 1.13 (d, J = 7 Hz, 9H), 1.47 (sept, J = 7 Hz, 3H), 3.13 (s, 6H), 6.72 (d, J = 9 Hz, 2H), 7.53 ppm (d, J = 9 Hz, 2H); ¹³C NMR (75 MHz, CDCl₃): δ = 12.42, 18.92, 18.95, 40.27, 74.85, 99.92, 110.94, 111.99, 112.98, 113.88, 114.14, 115.25, 131.67, 154.33, 169.58, 180.88 ppm; IR (neat): $\tilde{\nu}$ = 2959, 2874, 2212, 1769, 1740, 1698, 1592, 1486, 1431, 1391, 1336, 1294, 1239, 1209, 1167, 1086, 1069, 1038, 1006, 945, 929, 902, 872, 813 cm⁻¹; UV/Vis (CH₂Cl₂): λ (ϵ) = 252 (13500), 415 (sh, 15800), 454 nm (19700); HR-FT-MALDI-MS (DHB): m/z : calcd for C₂₅H₃₂N₅Si⁺: 430.2427; found: 430.2423 [$M+H$]⁺; elemental analysis calcd (%) for C₂₅H₃₁N₅Si (429.63): C 69.89, H 7.27, N 16.30; found: C 69.67, H 7.19, N 16.05.

2-[2-(Dimethylamino)phenyl]-3-(triisopropylsilyl)buta-1,3-diene-1,1,4,4-tetracarbonitrile (4): A mixture of **25** (100 mg, 0.332 mmol) and TCNE (44 mg, 0.34 mmol) was stirred for 30 min at 70°C. After cooling to 20°C, CC (CH₂Cl₂) afforded **4** (39 mg, 27%) as a red solid. ¹H NMR

(300 MHz, CDCl₃): δ = 0.93 (d, J = 8 Hz, 9H), 1.10 (d, J = 8 Hz, 9H), 1.45 (sept, J = 8 Hz, 3H), 2.65 (s, 6H), 7.31–7.62 ppm (m, 4H); IR (neat): $\tilde{\nu}$ = 2941, 2891, 2864, 2187, 2154, 1593, 1580, 1496, 1467, 1363, 1339, 1298, 1268, 1186, 1103, 1067, 995, 883, 814 cm⁻¹; HR-FT-MALDI-MS (3-HPA): m/z calcd for C₂₅H₃₂N₅Si⁺: 430.2427; found: 430.2430 [$M+H$]⁺.

2-[4-(Dimethylamino)-2-ethynylphenyl]ethylene-1,1,2-tricarbonitrile (5): A mixture of **26** (60 mg, 0.41 mmol) and TCNE (106 mg, 0.826 mmol) was stirred for 30 min at 70°C. After cooling to 20°C, CC (CH₂Cl₂) afforded **5** (70 mg, 69%) as a purple solid. M.p. 195–196°C; ¹H NMR (300 MHz, CDCl₃): δ = 3.15 (s, 6H), 3.57 (s, 1H), 6.72 (dd, J = 3, 9 Hz, 1H), 6.92 (d, J = 3 Hz, 1H), 7.58 ppm (d, J = 9 Hz, 1H); ¹³C NMR (75 MHz, CDCl₃): δ = 40.36, 80.48, 87.12, 89.42, 112.16, 112.40, 112.49, 113.83, 117.77, 117.85, 124.72, 132.53, 140.13, 153.51 ppm; IR (neat): $\tilde{\nu}$ = 3238, 2916, 2226, 2218, 2104, 1593, 1519, 1494, 1438, 1372, 1321, 1271, 1229, 1201, 1109, 1062, 956, 899, 863, 844, 807 cm⁻¹; UV/Vis (CH₂Cl₂): λ (ϵ) = 273 (12000), 333 (sh, 6000), 529 nm (22500); EI-MS (70 eV): m/z : 246 [M]⁺; elemental analysis calcd (%) for C₁₅H₁₀N₄ (246.27): C 73.16, H 4.09, N 22.75; found: C 72.15, H 4.07, N 22.37.

2-[4-(Dimethylamino)-2-[(triisopropylsilyl)ethynyl]phenyl]ethylene-1,1,2-tricarbonitrile (6): A mixture of **27** (113 mg, 0.375 mmol) and TCNE (95 mg, 0.74 mmol) was stirred for 30 min at 70°C. After cooling to 20°C, CC (CH₂Cl₂) afforded **6** (103 mg, 68%) as a purple solid. M.p. 70–71°C; ¹H NMR (300 MHz, CDCl₃): δ = 1.13–1.18 (m, 21H), 3.14 (s, 6H), 6.69 (dd, J = 3, 9 Hz, 1H), 6.86 (d, J = 3 Hz, 1H), 7.51 ppm (d, J = 9 Hz, 1H); ¹³C NMR (75 MHz, CDCl₃): δ = 11.42, 18.85, 40.33, 89.55, 102.72, 103.18, 111.78, 112.32, 112.51, 113.95, 117.55, 117.91, 126.09, 132.26, 140.52, 153.50 ppm; IR (neat): $\tilde{\nu}$ = 2944, 2864, 2226, 2216, 1592, 1486, 1376, 1323, 1269, 1218, 1201, 1119, 1064, 1017, 998, 970, 905, 882, 851, 805 cm⁻¹; UV/Vis (CH₂Cl₂): λ (ϵ) = 260 (17200), 275 (sh, 8000), 340 (sh, 3400), 384 (1300), 533 nm (15900); EI-MS (70 eV): m/z : 402 [M]⁺; HR-FT-MALDI-MS (3-HPA): m/z calcd for C₂₄H₃₁N₄Si⁺: 403.2318; found: 403.2320 [$M+H$]⁺; elemental analysis calcd (%) for C₂₄H₃₀N₄Si (402.61): C 71.60, H 7.51, N 13.92; found: C 71.89, H 7.61, N 13.67.

2-[[4-(Dimethylamino)phenyl]ethynyl]buta-1,3-diene-1,1,4,4-tetracarbonitrile (7): TCNE (76 mg, 0.59 mmol) was added to a solution of **28** (100 mg, 0.591 mmol) in CH₂Cl₂ (3 mL). The mixture was stirred for 1 h at 20°C. Evaporation and CC (CH₂Cl₂) afforded **7** (15 mg, 8.4%) as a blue solid. ¹H NMR (300 MHz, C₂D₂Cl₄): δ = 3.13 (s, 6H), 6.70 (d, J = 9 Hz, 2H), 7.64 (d, J = 9 Hz, 2H), 7.70 ppm (s, 1H); ¹³C NMR (75 MHz, C₂D₂Cl₄): δ = 40.38, 88.43, 88.80, 94.03, 105.11, 109.95, 112.04, 112.24, 112.41, 113.24, 128.05, 136.16, 139.76, 148.49, 153.33 ppm; IR (neat): $\tilde{\nu}$ = 2921, 2851, 2151, 1740, 1598, 1534, 1465, 1391, 1372, 1257, 1193, 1166, 1136, 972, 820 cm⁻¹; UV/Vis (CH₂Cl₂): λ (ϵ) = 290 (11800), 299 (12000), 367 (22000), 698 nm (12600); HR-FT-MALDI-MS (3-HPA): m/z calcd for C₁₈H₁₀N₅⁺: 296.0936; found: 296.0935 [$M-H$]⁺.

2-[4-(Dimethylamino)phenyl]-3-[(trimethylsilyl)ethynyl]buta-1,3-diene-1,1,4,4-tetracarbonitrile (8): TCNE (62 mg, 0.48 mmol) was added to a solution of **29** (116 mg, 0.481 mmol) in CH₂Cl₂ (5 mL). The mixture was stirred for 1 h at 20°C. Evaporation and CC (CH₂Cl₂) afforded **8** (26 mg, 15%) as a brown solid. M.p. 150–151°C (decomp); ¹H NMR (300 MHz, CDCl₃): δ = 0.31 (s, 9H), 3.18 (s, 6H), 6.74 (d, J = 10 Hz, 2H), 7.72 ppm (d, J = 10 Hz, 2H); ¹³C NMR (75 MHz, CDCl₃): δ = -0.76, 40.43, 74.43, 97.29, 97.83, 110.09, 111.15, 112.31, 113.27, 114.43, 117.55, 128.06, 132.60, 150.94, 154.73, 159.87 ppm; IR (neat): $\tilde{\nu}$ = 2901, 2214, 1607, 1552, 1494, 1439, 1385, 1349, 1307, 1249, 1214, 1174, 1064, 1023, 943, 845, 821 cm⁻¹; UV/Vis (CH₂Cl₂): λ (ϵ) = 302 (18700), 438 (23100), 457 nm (22900); ESI-MS: m/z : 370.2 [$M+H$]⁺; elemental analysis calcd (%) for C₂₁H₁₉N₅Si (369.49): C 68.26, H 5.18, N 18.95; found: C 68.62, H 4.72, N 18.96.

2-[4-(Dimethylamino)phenyl]-3-[(triisopropylsilyl)ethynyl]buta-1,3-diene-1,1,4,4-tetracarbonitrile (9): TCNE (118 mg, 0.921 mmol) was added to a solution of **30** (300 mg, 0.921 mmol) in CH₂Cl₂ (10 mL). The mixture was stirred for 1 h at 20°C. Evaporation and CC (CH₂Cl₂) afforded **9** (323 mg, 77%) as a black solid. M.p. 134.9–135.6°C; ¹H NMR (300 MHz, CDCl₃): δ = 1.07–1.22 (m, 21H), 3.17 (s, 6H), 6.73 (d, J = 9 Hz, 2H), 7.73 ppm (d, J = 9 Hz, 2H); ¹³C NMR (75 MHz, CDCl₃): δ = 11.25, 18.71, 40.44, 74.02, 96.82, 100.06, 110.20, 111.24, 112.32, 113.32, 114.43, 117.43, 126.74, 132.55, 150.97, 154.77, 160.22 ppm; IR (neat): $\tilde{\nu}$ = 2943, 2865, 2216, 2129, 1608, 1538, 1498, 1462, 1441, 1385, 1349, 1310,

1253, 1213, 1175, 1158, 1064, 1018, 997, 947, 918, 880, 817 cm⁻¹; UV/Vis (CH₂Cl₂): λ (ϵ) = 263 (14800), 312 (15500), 434 (22800), 469 (sh, 19600), 550 nm (sh, 6400); HR-FT-MALDI-MS (3-HPA): m/z calcd for C₂₇H₃₁N₅Si⁺: 453.2349; found: 453.2319 [M]⁺; elemental analysis calcd (%) for C₂₇H₃₁N₅Si (453.65): C 71.48, H 6.89, N 15.44; found: C 71.72, H 6.98, N 15.39.

2,3-Bis[4-(dimethylamino)phenyl]buta-1,3-diene-1,1,4,4-tetracarbonitrile (10): A solution of TCNE (24 mg, 0.19 mmol) in THF (2.0 mL) was added to a solution of **31** (50 mg, 0.19 mmol) in THF (5.0 mL). The mixture was stirred for 1 h at 20 °C. Filtration through a plug (CH₂Cl₂) followed by removal of the solvent in vacuo afforded **10** (76 mg, 100%) as a red solid. M.p. 273.5–274.6 °C; ¹H NMR (300 MHz, CDCl₃): δ = 3.14 (s, 12H), 6.69 (d, J = 9 Hz, 4H), 7.79 ppm (d, J = 9 Hz, 4H); ¹³C NMR (75 MHz, CDCl₃): δ = 40.14, 74.81, 111.85, 113.38, 114.59, 118.79, 132.44, 154.01, 165.38 ppm; IR (neat): $\tilde{\nu}$ = 3076, 2921, 2853, 2206, 1597, 1455, 1428, 1377, 1353, 1322, 1286, 1168, 1062, 942, 818 cm⁻¹; UV/Vis (CH₂Cl₂): λ (ϵ) = 278 (10400), 311 (sh, 5100), 323 (sh, 3400), 390 (sh, 17900), 470 nm (55000); HR-ESI-MS: m/z calcd for C₂₄H₂₁N₆⁺: 393.1828; found: 393.1822 [M+H]⁺, calcd for C₂₄H₂₀N₆Na⁺: 415.1647; found: 415.1635 [M+Na]⁺; elemental analysis calcd (%) for C₂₄H₂₀N₆ (392.46): C 73.45, H 5.14, N 21.41; found: C 70.99, H 5.18, N 20.00.

2-[4-(Dimethylamino)phenyl]-3-[4-(dimethylamino)phenyl]ethynyl]buta-1,3-diene-1,1,4,4-tetracarbonitrile (11): TCNE (114 mg, 0.890 mmol) was added to a solution of **32** (257 mg, 0.891 mmol) in CH₂Cl₂ (15 mL). The mixture was stirred for 2 h at 20 °C. Evaporation and CC (CH₂Cl₂) afforded **11** (354 mg, 96%) as a black solid. M.p. 191–193 °C; ¹H NMR (300 MHz, CDCl₃): δ = 3.10 (s, 6H), 3.15 (s, 6H), 6.64 (d, J = 9 Hz, 2H), 6.72 (d, J = 9 Hz, 2H), 7.48 (d, J = 9 Hz, 2H), 7.82 ppm (d, J = 9 Hz, 2H); ¹³C NMR (75 MHz, CDCl₃): δ = 40.29, 40.33, 74.38, 87.80, 90.42, 105.39, 111.71, 111.97, 112.12, 112.87, 113.55, 114.77, 117.93, 125.76, 132.70, 136.28, 150.15, 153.22, 154.53, 161.68 ppm; IR (neat): $\tilde{\nu}$ = 2917, 2217, 2122, 1598, 1538, 1479, 1435, 1372, 1329, 1295, 1210, 1171, 1113, 1063, 941, 808 cm⁻¹; UV/Vis (CH₂Cl₂): λ (ϵ) = 279 (13800), 430 (sh, 20800), 464 (sh, 25600), 526 nm (38100); HR-ESI-MS: m/z calcd for C₂₆H₂₁N₆⁺: 417.1828; found: 417.1822 [M+H]⁺; calcd for C₂₆H₂₀N₆Na⁺: 439.1647; found: 439.1637 [M+Na]⁺; elemental analysis calcd (%) for C₂₆H₂₀N₆ (416.48): C 74.98, H 4.84, N 20.18; found: C 74.98, H 4.90, N 20.12.

2-[2-(Dimethylamino)phenyl]-3-[3-(dimethylamino)phenyl]buta-1,3-diene-1,1,4,4-tetracarbonitrile (12): TCNE (7.0 mg, 0.055 mmol) was added to a solution of **33** (11.5 mg, 0.0435 mmol) in CH₂Cl₂ (1 mL). The mixture was stirred for 30 min at 20 °C. Evaporation and CC (CH₂Cl₂) afforded **12** (17.0 mg, 100%) as a red-brown solid. M.p. 185.9–186.6 °C; ¹H NMR (300 MHz, CDCl₃): δ = 2.72 (s, 6H), 2.92 (s, 6H), 6.53–7.21 (m, 6H), 7.48 (dt, J = 2, 8 Hz, 1H), 7.55 ppm (dd, J = 2, 8 Hz, 1H); ¹³C NMR (75 MHz, CDCl₃): δ = 40.42, 46.09, 87.65, 89.94, 111.71, 111.80, 112.39, 112.61, 112.89, 116.71, 116.84, 121.35, 124.72, 128.89, 129.93, 132.81, 132.94, 135.22, 150.43, 154.22, 167.24, 169.77 ppm; IR (neat): $\tilde{\nu}$ = 2865, 2223, 1592, 1567, 1549, 1528, 1487, 1454, 1427, 1369, 1326, 1307, 1239, 1183, 1162, 1143, 1071, 1045, 1001, 944, 842 cm⁻¹; UV/Vis (CH₂Cl₂): λ (ϵ) = 260 (29200), 342 (8800), 481 nm (2500); EI-MS (70 eV): m/z : 392 [M]⁺; elemental analysis calcd (%) for C₂₄H₂₀N₆ (392.46): C 73.45, H 5.14, N 21.41; found: C 72.27, H 5.28, N 20.63.

2-(4-Methoxyphenyl)buta-1,3-diene-1,1,4,4-tetracarbonitrile (13): TCNE (291 mg, 2.27 mmol) was added to a solution of **34** (300 mg, 2.27 mmol) in C₆H₆ (11 mL). The mixture was heated to reflux for 5 h. After cooling to 20 °C, the solution was passed through a plug (CH₂Cl₂) and the filtrate was evaporated. Preparative GPC (CH₂Cl₂) afforded **13** (190 mg, 32%) as an orange solid. M.p. 181.5–183.4 °C; ¹H NMR (300 MHz, CDCl₃): δ = 3.92 (s, 3H), 7.09 (d, J = 9 Hz, 2H), 7.45 (d, J = 9 Hz, 2H), 8.02 ppm (s, 1H); ¹³C NMR (75 MHz, CDCl₃): δ = 55.85, 88.91, 98.04, 108.40, 111.13, 111.52, 111.69, 115.64, 122.22, 131.33, 153.21, 161.24, 164.43 ppm; IR (neat): $\tilde{\nu}$ = 3047, 2851, 2224, 1602, 1534, 1507, 1463, 1348, 1315, 1257, 1181, 1018, 837 cm⁻¹; UV/Vis (CH₂Cl₂): λ (ϵ) = 288 (24100), 446 nm (6200); EI-MS (70 eV): m/z : 260 [M]⁺; elemental analysis calcd (%) for C₁₅H₈N₄O (260.25): C 69.23, H 3.10, N 21.53, O 6.15; found: C 69.08, H 3.27, N 21.51, O 6.32.

2,3-Bis(4-methoxyphenyl)buta-1,3-diene-1,1,4,4-tetracarbonitrile (14): TCNE (96 mg, 0.75 mmol) was added to a solution of **35** (178 mg,

0.747 mmol) in toluene (10 mL). The mixture was heated to reflux for 12 h. After cooling to 20 °C, the solvent was evaporated. CC (CH₂Cl₂) afforded **14** (116 mg, 42%) as a yellow solid. M.p. 213.4–213.9 °C; ¹H NMR (300 MHz, CDCl₃): δ = 3.92 (s, 6H), 7.04 (d, J = 9 Hz, 4H), 7.77 ppm (d, J = 9 Hz, 4H); ¹³C NMR (75 MHz, CDCl₃): δ = 55.97, 82.92, 111.64, 112.48, 115.53, 123.58, 132.02, 164.80, 166.15 ppm; IR (neat): $\tilde{\nu}$ = 2933, 2844, 2224, 1598, 1568, 1532, 1504, 1457, 1438, 1344, 1312, 1272, 1253, 1193, 1173, 1122, 1021, 848, 836 cm⁻¹; UV/Vis (CH₂Cl₂): λ (ϵ) = 327 (sh, 18900), 380 nm (29300); EI-MS (70 eV): m/z : 366 [M]⁺; elemental analysis calcd (%) for C₂₂H₁₄N₄O₂ (366.37): C 72.12, H 3.85, N 15.29; found: C 69.68, H 3.93, N 14.63.

2-(4-Methoxyphenyl)-3-[(4-methoxyphenyl)ethynyl]buta-1,3-diene-1,1,4,4-tetracarbonitrile (15): A mixture of **36** (208 mg, 0.792 mmol) and TCNE (102 mg, 0.796 mmol) was stirred for 10 min at 170 °C. After cooling to 20 °C, CC (CH₂Cl₂) afforded **15** (36 mg, 12%) as an orange solid. M.p. 52–54 °C; ¹H NMR (300 MHz, CDCl₃): δ = 3.88 (s, 3H), 3.93 (s, 3H), 6.95 (d, J = 9 Hz, 2H), 7.07 (d, J = 9 Hz, 2H), 7.59 (d, J = 9 Hz, 2H), 7.79 ppm (d, J = 9 Hz, 2H); ¹³C NMR (75 MHz, CDCl₃): δ = 55.79, 56.00, 82.98, 86.62, 92.36, 110.36, 110.96, 111.55, 112.45, 114.95, 115.46, 120.96, 123.01, 132.01, 135.95, 148.96, 162.59, 163.53, 164.88 ppm; IR (neat): $\tilde{\nu}$ = 2924, 2851, 2228, 2155, 1738, 1598, 1568, 1505, 1462, 1362, 1301, 1256, 1172, 1120, 1021, 833, 802 cm⁻¹; UV/Vis (CH₂Cl₂): λ (ϵ) = 332 (17400), 425 nm (25900); EI-MS (70 eV): m/z : 390 [M]⁺; elemental analysis calcd (%) for C₂₄H₁₄N₄O₂ (390.39): C 73.84, H 3.61, N 14.35; found: C 73.84, H 3.56, N 14.07.

2-Phenyl-3-(2-thienyl)buta-1,3-diene-1,1,4,4-tetracarbonitrile (16): A mixture of **37** (115 mg, 0.624 mmol) and TCNE (240 mg, 1.87 mmol) was stirred for 8 h at 150 °C. After cooling to 20 °C, CC (CH₂Cl₂) afforded **16** (155 mg, 80%) as a red solid. M.p. 207.8–208.3 °C; ¹H NMR (300 MHz, C₂D₂Cl₄): δ = 7.35 (dd, J = 4, 5 Hz, 1H), 7.58–7.76 (m, 5H), 7.88 (dd, J = 1, 4 Hz, 1H), 8.05 ppm (dd, J = 1, 5 Hz, 1H); ¹³C NMR (75 MHz, C₂D₂Cl₄): δ = 73.84, 79.52, 87.08, 110.70, 111.29, 112.11, 128.93, 129.86, 130.04, 130.28, 133.93, 134.85, 137.38, 138.83, 157.45, 166.27 ppm; IR (neat): $\tilde{\nu}$ = 3097, 2948, 2229, 1592, 1576, 1532, 1493, 1444, 1401, 1364, 1347, 1257, 1236, 1207, 1180, 1110, 1068, 1030, 999, 869, 847, 826 cm⁻¹; UV/Vis (CH₂Cl₂): λ (ϵ) = 316 (17500), 366 nm (15800); EI-MS (70 eV): m/z : 312 [M]⁺; elemental analysis calcd (%) for C₁₈H₈N₄S (312.35): C 69.22, H 2.58, N 17.94; found: C 66.96, H 2.49, N 16.94.

2,3-Di-2-thienylbuta-1,3-diene-1,1,4,4-tetracarbonitrile (17): A mixture of **38** (80 mg, 0.42 mmol) and TCNE (162 mg, 1.26 mmol) was stirred for 14 h at 150 °C. After cooling to 20 °C, CC (CH₂Cl₂) afforded **17** (107 mg, 80%) as an orange solid. M.p. 202.4–204.0 °C; ¹H NMR (300 MHz, CDCl₃): δ = 7.31 (dd, J = 4, 5 Hz, 2H), 7.86 (dd, J = 1, 4 Hz, 2H), 7.99 ppm (dd, J = 1, 5 Hz, 2H); ¹³C NMR (75 MHz, CDCl₃): δ = 80.62, 111.23, 112.22, 129.97, 134.32, 137.51, 138.56, 156.93 ppm; IR (neat): $\tilde{\nu}$ = 3081, 2948, 2224, 1523, 1403, 1341, 1240, 1071, 1006, 862 cm⁻¹; UV/Vis (CH₂Cl₂): λ (ϵ) = 315 (16900), 369 nm (30100); EI-MS (70 eV): m/z : 318 [M]⁺; elemental analysis calcd (%) for C₁₆H₆N₄S₂ (318.38): C 60.36, H 1.90, N 17.60; found: C 60.06, H 1.90, N 17.46.

2-[4-{3,3-Dicyano-1-(dicyanomethylene)-2-[4-(dihexylamino)phenyl]prop-2-en-1-yl}phenyl]-3-[4-(dihexylamino)phenyl]buta-1,3-diene-1,1,4,4-tetracarbonitrile (18): TCNE (30 mg, 0.23 mmol) was added to a solution of **39** (50 mg, 0.078 mmol) in CH₂Cl₂ (5 mL). The mixture was stirred for 3 h at 20 °C. Evaporation and CC (CH₂Cl₂) afforded **18** (70 mg, 99%) as a dark brown solid. M.p. 232–234 °C; ¹H NMR (300 MHz, CDCl₃): δ = 0.91 (t, J = 7 Hz, 12H), 1.35 (m, 24H), 1.65 (m, 8H), 3.41 (t, J = 8 Hz, 8H), 6.72 (d, J = 9 Hz, 4H), 7.78 (d, J = 9 Hz, 4H), 7.82 ppm (s, 4H); ¹³C NMR (75 MHz, CDCl₃): δ = 14.22, 22.83, 26.87, 27.54, 31.73, 51.83, 72.15, 90.11, 110.97, 111.57, 112.87, 114.15, 114.55, 116.72, 130.47, 133.01, 136.24, 153.66, 160.87, 167.47 ppm; IR (neat): $\tilde{\nu}$ = 2926, 2856, 2213, 1602, 1532, 1483, 1446, 1415, 1343, 1298, 1260, 1214, 1183, 1118, 1015, 977, 891, 819 cm⁻¹; UV/Vis (CH₂Cl₂): λ (ϵ) = 254 (24900), 281 (21600), 346 (31700), 476 nm (99900); HR-FT-MALDI-MS (DHB): m/z : calcd for C₅₈H₆₅N₁₀⁺: 901.5394; found: 901.5372 [M+H]⁺; calcd for C₅₈H₆₄N₁₀Na⁺: 923.5213; found: 923.5258 [M+Na]⁺; elemental analysis calcd (%) for C₅₈H₆₄N₁₀ (901.20): C 77.30, H 7.16, N 15.54; found: C 77.37, H 7.01, N 15.26.

2-[4-(Dihexylamino)phenyl]-3-[2-[[4-(dihexylamino)phenyl]ethynyl]phenyl]buta-1,3-diene-1,1,4,4-tetracarboxitrile (19): TCNE (26 mg, 0.20 mmol) was added to a solution of **40** (132 mg, 0.21 mmol) in CH₂Cl₂ (13 mL). The mixture was stirred for 3 h at 20 °C. Evaporation and CC (CH₂Cl₂) afforded **19** (61 mg, 39%) as a dark yellow solid. M.p. 43–45 °C; ¹H NMR (300 MHz, CD₂Cl₂): δ = 0.92 (t, *J* = 7 Hz, 12H), 1.34 (m, 24H), 1.56–1.65 (m, 8H), 3.29 (t, *J* = 8 Hz, 4H), 3.38 (t, *J* = 8 Hz, 4H), 6.61 (brs, 2H), 6.65 (d, *J* = 9 Hz, 2H), 6.84 (dd, *J* = 2, 6 Hz, 1H), 7.06 (brs, 2H), 7.29–7.40 (m, 2H), 7.82 (d, *J* = 9 Hz, 2H), 8.29 ppm (dd, *J* = 2, 6 Hz, 1H); ¹³C NMR (75 MHz, CD₂Cl₂): δ = 14.00, 14.04, 22.85, 22.93, 26.82, 26.99, 27.25, 27.36, 31.80, 31.91, 51.10, 51.41, 73.24, 82.90, 111.29, 111.67, 113.95, 115.10, 115.64, 118.08, 121.82, 126.17, 128.82, 132.21, 132.64, 133.98, 141.30, 143.15, 146.23, 149.65, 152.83, 162.43, 164.60 ppm; IR (neat): $\tilde{\nu}$ = 2926, 2855, 2214, 1599, 1516, 1486, 1456, 1411, 1354, 1322, 1296, 1257, 1178, 1105, 816 cm⁻¹; UV/Vis (CH₂Cl₂): λ (ε) = 278 (21 400), 312 (24 100), 442 nm (30 000); HR-FT-MALDI-MS (3-HPA): *m/z*: calcd for C₅₂H₆₅N₆⁺: 773.5271; found: 773.5252 [*M*+H]⁺; elemental analysis calcd (%) for C₅₂H₆₄N₆ (773.10): C 80.79, H 8.34, N 10.87; found: C 80.68, H 8.46, N 10.57.

3,3'-(1,3-Phenylene)bis[2-[4-(dihexylamino)phenyl]buta-1,3-diene-1,1,4,4-tetracarboxitrile (20): TCNE (71 mg, 0.55 mmol) was added to a solution of **41** (118 mg, 0.183 mmol) in CH₂Cl₂ (12 mL). The mixture was stirred for 3 h at 20 °C. Evaporation and CC (CH₂Cl₂) afforded **20** (142 mg, 86%) as a dark red solid. M.p. 75–79 °C; ¹H NMR (300 MHz, CDCl₃): δ = 0.92 (t, *J* = 7 Hz, 12H), 1.35 (m, 24H), 1.65 (m, 8H), 3.41 (t, *J* = 8 Hz, 8H), 6.70 (d, *J* = 10 Hz, 4H), 7.70–7.76 (m, 6H), 8.01 ppm (d, *J* = 8 Hz, 2H); ¹³C NMR (75 MHz, CDCl₃): δ = 14.17, 22.70, 26.72, 27.37, 31.58, 51.63, 71.94, 89.66, 110.60, 111.30, 112.56, 112.65, 113.84, 114.25, 116.37, 130.38, 131.08, 132.59, 133.24, 153.27, 160.42, 167.28 ppm; IR (neat): $\tilde{\nu}$ = 2926, 2856, 2212, 1600, 1483, 1445, 1414, 1341, 1296, 1213, 1182, 1117, 976, 891, 819 cm⁻¹; UV/Vis (CH₂Cl₂): λ (ε) = 273 (27 800), 307 (30 400), 460 (54 500), 466 nm (54 200); HR-FT-MALDI-MS (DHB): *m/z*: calcd for C₅₈H₆₅N₁₀⁺: 901.5394; found: 901.5297 [*M*+H]⁺; calcd for C₅₈H₆₄N₁₀Na⁺: 923.5213; found: 923.5197 [*M*+Na]⁺; elemental analysis calcd (%) for C₅₈H₆₄N₁₀ (901.20): C 77.30, H 7.16, N 15.54; found: C 77.42, H 7.05, N 15.49.

3,3',3''-Benzene-1,3,5-triyltris[2-[4-(dihexylamino)phenyl]buta-1,3-diene-1,1,4,4-tetracarboxitrile (21): TCNE (50 mg, 0.39 mmol) was added to a solution of **42** (80 mg, 0.086 mmol) in CH₂Cl₂ (10 mL). The mixture was stirred for 3 h at 20 °C. Evaporation and CC (CH₂Cl₂) afforded **21** (97 mg, 86%) as a dark brown solid. M.p. 88–90 °C; ¹H NMR (300 MHz, CDCl₃): δ = 0.92 (t, *J* = 7 Hz, 18H), 1.36 (m, 36H), 1.67 (m, 12H), 3.43 (t, *J* = 8 Hz, 12H), 6.74 (d, *J* = 9 Hz, 6H), 7.72 (d, *J* = 9 Hz, 6H), 8.01 ppm (s, 3H); ¹³C NMR (75 MHz, CDCl₃): δ = 14.23, 22.83, 26.87, 27.54, 31.73, 51.90, 72.34, 91.82, 110.37, 111.13, 113.28, 114.21, 114.29, 116.80, 132.97, 133.54, 135.02, 153.87, 159.69, 166.37 ppm; IR (neat): $\tilde{\nu}$ = 2926, 2855, 2212, 1601, 1483, 1445, 1415, 1339, 1296, 1212, 1183, 1103, 979, 888, 822 cm⁻¹; UV/Vis (CH₂Cl₂): λ (ε) = 254 (41 400), 292 (47 100), 463 (90 700), 590 nm (sh, 16 500); HR-FT-MALDI-MS (3-HPA): *m/z*: calcd for C₈₄H₉₃N₁₅Na⁺: 1334.764; found: 1334.760 [*M*+Na]⁺; elemental analysis calcd (%) for C₈₄H₉₃N₁₅ (1312.74): C 76.86, H 7.14, N 16.00; found: C 76.84, H 7.02, N 15.82.

Acknowledgements

This research was supported by the ETH Research Council and the Fonds der Chemischen Industrie (Germany). We thank Prof. P. Walde, M. Colussi, and F. Choffat for the TGA measurements.

- [1] a) P. N. Prasad, D. J. Williams, *Introduction to Nonlinear Optical Effects in Molecules and Polymers*, Wiley, New York, **1991**; b) J. L. Brédas, C. Adant, P. Tackx, A. Persoons, B. M. Pierce, *Chem. Rev.* **1994**, *94*, 243–278; c) S. R. Marder, B. Kippelen, A. K.-Y. Jen, N. Peyghambarian, *Nature* **1997**, *388*, 845–851; d) U. Gubler, C. Bosshard, *Adv. Polym. Sci.* **2002**, *158*, 123–191; e) L. R. Dalton, *J. Phys. Condens. Matter* **2003**, *15*, R897–R934.

- [2] a) S. R. Marder, J. W. Perry, G. Bourhill, C. B. Gorman, B. G. Tie-mann, K. Mansour, *Science* **1993**, *261*, 186–189; b) F. Meyers, S. R. Marder, B. M. Pierce, J. L. Brédas, *J. Am. Chem. Soc.* **1994**, *116*, 10703–10714; c) R. R. Tykwinski, M. Schreiber, V. Gramlich, P. Seiler, F. Diederich, *Adv. Mater.* **1996**, *8*, 226–231; d) R. Spreiter, C. Bosshard, G. Knöpfle, P. Günter, R. R. Tykwinski, M. Schreiber, F. Diederich, *J. Phys. Chem. B* **1998**, *102*, 29–32; e) R. R. Tykwinski, U. Gubler, R. E. Martin, F. Diederich, C. Bosshard, P. Günter, *J. Phys. Chem. B* **1998**, *102*, 4451–4465.
- [3] a) C. Bosshard, R. Spreiter, P. Günter, R. R. Tykwinski, M. Schreiber, F. Diederich, *Adv. Mater.* **1996**, *8*, 231–234; b) U. Gubler, R. Spreiter, C. Bosshard, P. Günter, R. R. Tykwinski, F. Diederich, *Appl. Phys. Lett.* **1998**, *73*, 2396–2398.
- [4] a) N. N. P. Moonen, R. Gist, C. Boudon, J.-P. Gisselbrecht, P. Seiler, T. Kawai, A. Kishioka, M. Gross, M. Irie, F. Diederich, *Org. Biomol. Chem.* **2003**, *1*, 2032–2034; b) N. N. P. Moonen, W. C. Pom-erantz, R. Gist, C. Boudon, J.-P. Gisselbrecht, T. Kawai, A. Kishioka, M. Gross, M. Irie, F. Diederich, *Chem. Eur. J.* **2005**, *11*, 3325–3341; c) J. C. May, J. H. Lim, I. Biaggio, N. N. P. Moonen, T. Michi-nobu, F. Diederich, *Opt. Lett.* **2005**, *30*, 3057–3059.
- [5] a) A. J. Fatiadi, *Synthesis* **1986**, 249–284; b) A. J. Fatiadi, *Synthesis* **1987**, 749–789; c) O. W. Webster, *J. Polym. Sci. Part A* **2002**, *40*, 210–221.
- [6] N. N. P. Moonen, C. Boudon, J.-P. Gisselbrecht, P. Seiler, M. Gross, F. Diederich, *Angew. Chem.* **2002**, *114*, 3170–3173; *Angew. Chem. Int. Ed.* **2002**, *41*, 3044–3047.
- [7] For a preliminary communication of parts of this work, including some first NLO data, see: T. Michinobu, J. C. May, J. H. Lim, C. Boudon, J.-P. Gisselbrecht, P. Seiler, M. Gross, I. Biaggio, F. Dieder-ich, *Chem. Commun.* **2005**, 737–739.
- [8] B. M. Trost, *Science* **1991**, *254*, 1471–1477.
- [9] a) C. Cai, I. Liakatas, M.-S. Wong, M. Bösch, C. Bosshard, P. Günter, S. Concilio, N. Tirelli, U. W. Suter, *Org. Lett.* **1999**, *1*, 1847–1849; b) H. Ma, A. K.-Y. Jen, J. Wu, X. Wu, S. Liu, C.-F. Shu, L. R. Dalton, S. R. Marder, S. Thayumanavan, *Chem. Mater.* **1999**, *11*, 2218–2225; c) X. Wu, J. Wu, Y. Liu, A. K.-Y. Jen, *J. Am. Chem. Soc.* **1999**, *121*, 472–473; d) H. Ma, B. Chen, T. Sassa, L. R. Dalton, A. K.-Y. Jen, *J. Am. Chem. Soc.* **2001**, *123*, 986–987; e) A. Galvan-Gonzalez, G. I. Stegeman, A. K.-Y. Jen, X. Wu, M. Canva, A. C. Ko-walczyk, X. Q. Zhang, H. S. Lackritz, S. Marder, S. Thayumanavan, G. Levina, *J. Opt. Soc. Am. B* **2001**, *18*, 1846–1853; f) J. Luo, H. Ma, M. Haller, A. K.-Y. Jen, R. R. Barto, *Chem. Commun.* **2002**, 888–889; g) Y. V. Pereverzev, O. V. Prezhdo, L. R. Dalton, *Chem. Phys. Lett.* **2003**, *373*, 207–212; h) V. Mamane, I. Ledoux-Rak, S. Deveau, J. Zyss, O. Riant, *Synthesis* **2003**, 455–467; i) Y. Morioka, N. Yoshi-zawa, J.-i. Nishida, Y. Yamashita, *Chem. Lett.* **2004**, *33*, 1190–1191.
- [10] a) M. I. Bruce, J. R. Rodgers, M. R. Snow, A. G. Swincer, *J. Chem. Soc. Chem. Commun.* **1981**, 271–272; b) M. I. Bruce, T. W. Hambley, M. R. Snow, A. G. Swincer, *Organometallics* **1985**, *4*, 494–500; c) M. I. Bruce, M. Ke, P. J. Low, B. W. Skelton, A. H. White, *Orga-nometallics* **1998**, *17*, 3539–3549; d) M. I. Bruce, B. C. Hall, B. D. Kelly, P. J. Low, B. W. Skelton, A. H. White, *J. Chem. Soc. Dalton Trans.* **1999**, 3719–3728; e) M. I. Bruce, M. E. Smith, B. W. Skelton, A. H. White, *J. Organomet. Chem.* **2001**, *637*–639, 484–499; f) K. Onitsuka, S. Takahashi, *J. Chem. Soc. Chem. Commun.* **1995**, 2095–2096; g) Y. Yamamoto, R. Satoh, T. Tanase, *J. Chem. Soc. Dalton Trans.* **1995**, 307–311; h) K. Onitsuka, N. Ose, F. Ozawa, S. Takaha-shi, *J. Organomet. Chem.* **1999**, *578*, 169–177; i) T. Mochida, S. Ya-mazaki, *J. Chem. Soc. Dalton Trans.* **2002**, 3559–3564.
- [11] a) M. Albota, D. Beljonne, J.-L. Brédas, J. E. Ehrlich, J.-Y. Fu, A. A. Heikal, S. E. Hess, T. Kogej, M. D. Levin, S. R. Marder, D. McCord-Maughon, J. W. Perry, H. Röckel, M. Rumi, G. Subramaniam, W. W. Webb, X.-L. Wu, C. Xu, *Science* **1998**, *281*, 1653–1656; b) B. R. Cho, M. J. Piao, K. H. Son, S. H. Lee, S. J. Yoon, S.-J. Jeon, M. Cho, *Chem. Eur. J.* **2002**, *8*, 3907–3916.
- [12] E. A. Meyer, R. K. Castellano, F. Diederich, *Angew. Chem.* **2003**, *115*, 1244–1287; *Angew. Chem. Int. Ed.* **2003**, *42*, 1210–1250.

- [13] For a recent review on multipolar interactions, see: R. Paulini, K. Müller, F. Diederich, *Angew. Chem.* **2005**, *117*, 1820–1839; *Angew. Chem. Int. Ed.* **2005**, *44*, 1788–1805.
- [14] a) C. Dehu, F. Meyers, J. L. Brédas, *J. Am. Chem. Soc.* **1993**, *115*, 6198–6206; b) A. Hilger, J.-P. Gisselbrecht, R. R. Tykwinski, C. Boudon, M. Schreiber, R. E. Martin, H. P. Lüthi, M. Gross, F. Diederich, *J. Am. Chem. Soc.* **1997**, *119*, 2069–2078.
- [15] N. N. P. Moonen, F. Diederich, *Org. Biomol. Chem.* **2004**, *2*, 2263–2266.
- [16] T. Mizoguchi, R. N. Adams, *J. Am. Chem. Soc.* **1962**, *84*, 2058–2061.
- [17] a) H. Meier, B. Mühling, H. Kolshorn, *Eur. J. Org. Chem.* **2004**, 1033–1042; b) H. Meier, J. Gerold, H. Kolshorn, B. Mühling, *Chem. Eur. J.* **2004**, *10*, 360–370; c) H. Meier, *Angew. Chem.* **2005**, *117*, 2536–2561; *Angew. Chem. Int. Ed.* **2005**, *44*, 2482–2506.
- [18] P. Zuman, *Substituent Effects in Organic Polarography*, Plenum Press, New York, **1967**.
- [19] C. Diaz, A. Arancibia, *Polyhedron* **2000**, *19*, 137–145.
- [20] D. H. Evans, K. M. O'Connell, *Electroanalytical Chemistry*, Vol. 14, (Ed.: A. J. Bard), Marcel Dekker, New York, **1986**, pp. 113–207.
- [21] a) P. Suppan, N. Ghoneim, *Solvatochromism*, The Royal Society of Chemistry, Cambridge, **1997**; b) P. Suppan, *J. Photochem. Photobiol. A* **1990**, *50*, 293–330.
- [22] a) N. Ghoneim, P. Suppan, *Spectrochim. Acta Part A* **1995**, *51*, 1043–1050; b) B. Strehmel, A. M. Sarker, H. Detert, *ChemPhysChem* **2003**, *4*, 249–259.
- [23] a) A. D. Becke, *J. Chem. Phys.* **1993**, *98*, 5648–5652; b) C. Lee, W. Yang, R. G. Parr, *Phys. Rev. B* **1988**, *37*, 785–789.
- [24] Gaussian 98, Revision A.7, M. J. Frisch, G. W. Trucks, H. B. Schlegel, G. E. Scuseria, M. A. Robb, J. R. Cheeseman, V. G. Zakrzewski, J. A. Montgomery, Jr., R. E. Stratmann, J. C. Burant, S. Dapprich, J. M. Millam, A. D. Daniels, K. N. Kudin, M. C. Strain, O. Farkas, J. Tomasi, V. Barone, M. Cossi, R. Cammi, B. Mennucci, C. Pomelli, C. Adamo, S. Clifford, J. Ochterski, G. A. Petersson, P. Y. Ayala, Q. Cui, K. Morokuma, D. K. Malick, A. D. Rabuck, K. Raghavachari, J. B. Foresman, J. Cioslowski, J. V. Ortiz, B. B. Stefanov, G. Liu, A. Liashenko, P. Piskorz, I. Komaromi, R. Gomperts, R. L. Martin, D. J. Fox, T. Keith, M. A. Al-Laham, C. Y. Peng, A. Nanayakkara, C. Gonzales, M. Challacombe, P. M. W. Gill, B. G. Johnson, C. Gonzalez, W. Chen, M. W. Wong, J. L. Andres, M. Head-Gordon, E. S. Replogle, J. A. Pople, Gaussian Inc., Pittsburgh, PA, **1998**.
- [25] Spartan'04, Wavefunction, Inc. Irvine, CA, **2003**.
- [26] The successful synthesis of some potential precursor polymers was recently reported: a) W. Zhang, J. S. Moore, *Macromolecules* **2004**, *37*, 3973–3975; b) S. W. Thomas, III, T. M. Swager, *Macromolecules* **2005**, *38*, 2716–2721.
- [27] a) C. A. Thomas, K. Zong, K. A. Abboud, P. J. Steel, J. R. Reynolds, *J. Am. Chem. Soc.* **2004**, *126*, 16440–16450; b) A. Berlin, G. Zotti, S. Zecchin, G. Schiavon, B. Vercelli, A. Zanelli, *Chem. Mater.* **2004**, *16*, 3667–3676.
- [28] For another, recently reported interesting family of cruciform-shaped D–A chromophores, see: a) J. N. Wilson, M. Josowicz, Y. Wang, U. H. F. Bunz, *Chem. Commun.* **2003**, 2962–2963; b) J. N. Wilson, U. H. F. Bunz, *J. Am. Chem. Soc.* **2005**, *127*, 4124–4125.
- [29] Thin-film preparation by vapor deposition techniques and its application in nanosciences were successful for donor-substituted CEEs: G. Jiang, T. Michinobu, W. Yuan, M. Feng, Y. Wen, S. Du, H. Gao, L. Jiang, Y. Song, F. Diederich, D. Zhu, *Adv. Mater.* **2005**, *17*, 2170–2173.
- [30] K. A. Leonard, M. I. Nelen, L. T. Anderson, S. L. Gibson, R. Hilf, M. R. Detty, *J. Med. Chem.* **1999**, *42*, 3942–3952.
- [31] J. Szewczyk, A. Gryff-Keller, *J. Organomet. Chem.* **1992**, *424*, 41–47.
- [32] J. G. Rodríguez, A. Lafuente, R. Martín-Villamil, M. P. Martínez-Alcazar, *J. Phys. Org. Chem.* **2001**, *14*, 859–868.
- [33] A. P. Rudenko, A. V. Vasil'ev, *Russ. J. Org. Chem.* **1995**, *31*, 1360–1379.
- [34] W. Zhang, S. Kraft, J. S. Moore, *J. Am. Chem. Soc.* **2004**, *126*, 329–335.
- [35] W. Schroth, S. Dunger, F. Billig, R. Spitzner, R. Herzsuh, A. Vogt, T. Jende, G. Israel, J. Barche, D. Ströhl, J. Sieler, *Tetrahedron* **1996**, *52*, 12677–12698.
- [36] H.-G. Kim, J.-K. Lee, J.-T. Lee, C.-S. Lee, *Bull. Korean Chem. Soc.* **2000**, *21*, 345–347.
- [37] M. J. Mio, L. C. Kopel, J. B. Braun, T. L. Gadzikwa, K. L. Hull, R. G. Brisbois, C. J. Markworth, P. A. Grieco, *Org. Lett.* **2002**, *4*, 3199–3202.
- [38] F. Mitzel, C. Boudon, J.-P. Gisselbrecht, P. Seiler, M. Gross, F. Diederich, *Helv. Chim. Acta* **2004**, *87*, 1130–1157.
- [39] R. F. Kubin, A. N. Fletcher, *J. Lumin.* **1982**, *27*, 455–462.
- [40] G. G. Guilbault, *Practical Fluorescence*, 2nd ed., Marcel Dekker, New York, **1990**.
- [41] A. Altomare, M. C. Burla, M. Camalli, G. L. Cascarano, C. Giacovazzo, A. Guagliardi, A. G. G. Moliterni, G. Polidori, R. Spagna, *J. Appl. Crystallogr.* **1999**, *32*, 115–119.
- [42] G. M. Sheldrick, SHELXL-97, Program for the Refinement of Crystal Structures, University of Göttingen, Germany, **1997**.

Received: September 8, 2005
Published online: January 3, 2006